Latest Jurassic–earliest Cretaceous closure of the Mongol-Okhotsk Ocean: A paleomagnetic and seismological-tomographic analysis

Rob Van der Voo*

Department of Earth and Environmental Sciences, University of Michigan, Ann Arbor, Michigan 48109, USA

Douwe J.J. van Hinsbergen

Department of Earth Sciences, Utrecht University, Budapestlaan 4, 3584 CD Utrecht, the Netherlands

Mathew Domeier

Physics of Geological Processes (PGP), University of Oslo, Sem Sælands vei 24, NO-0316 Oslo, Norway, and
Center for Earth Evolution and Dynamics (CEED), University of Oslo, Sem Sælands vei 24, NO-0316 Oslo, Norway

Wim Spakman

Department of Earth Sciences, Utrecht University, Budapestlaan 4, 3584 CD Utrecht, the Netherlands, and
Center for Earth Evolution and Dynamics (CEED), University of Oslo, Sem Sælands vei 24, NO-0316 Oslo, Norway

Trond H. Torsvik

Physics of Geological Processes (PGP), University of Oslo, Sem Sælands vei 24, NO-0316 Oslo, Norway, and
Center for Earth Evolution and Dynamics (CEED), University of Oslo, Sem Sælands vei 24, NO-0316 Oslo, Norway, and
School of Geosciences, University of the Witwatersrand, Wits 2050, South Africa

ABSTRACT

The Mongol-Okhotsk Ocean closed when the Amuria block, normally considered to have been part of the North China block since the early Mesozoic, and the southern margin of Siberia collided in Late Jurassic to Early Cretaceous times. The resulting suture runs WSW-ENE and is reasonably well defined to the east of longitude 100°E. Because no evidence exists for any westward prolongation of the Mongol-Okhotsk Ocean suture toward the Tarim block, the cryptic termination of the suture is an enigma, compounded by the fact that a tomographically identified slab in the lower 1000 km of the mantle, interpreted as a remnant of Mongol-Okhotsk oceanic lithosphere, has a clear N-S trend, at almost right angles to the surface suture. No sensible explanation can be constructed for a rotation of some 90° of this slab. There is a solution, however, to both these enigmas if we consider that the Triassic Mongol-Okhotsk Ocean existed east of an initially meridian-parallel, but later progressively

*Corresponding author; e-mail: voo@umich.edu

more sinuous, late Paleozoic Pangea margin. This margin consisted of Siberia, Amuria, and the China continental elements. The Mongol-Okhotsk Ocean was subducting westward during the early Mesozoic and likely older times underneath this margin. This would readily explain the tomographic N-S slab orientation at depths of 2000 km and greater. Paleomagnetic inclination differences between the global apparent polar wander path in Siberian coordinates and results from the North China block show a gradually diminishing trend with time, as these cratons approached each other during the Jurassic. During this time, the paleomagnetic data of the North China block show that it underwent a slight northward motion, but with a considerable counterclockwise rotation of ~90°. At the same time, the Mongol-Okhotsk Ocean–bordering margin of Eurasia (between Siberia and Tarim) moved southward by ~30° and rotated 45° clockwise. These continental scissoring movements caused doubly vergent subduction of the Mongol-Okhotsk Ocean. Paleomagnetic data suggest final closure of the Mongol-Okhotsk Ocean in latest Jurassic–earliest Cretaceous time. Arc-related rocks above the subduction zone follow the outline around the core of the Tuva-Mongol belt in the eastern Altaids between Amuria and Siberia, and they form a tightening, westward-convex Tuva-Mongol orocline. This large-scale oroclinal bending of the crust above a disappearing ocean is reminiscent of similarly tightening oroclines in Kazakhstan and Variscan Europe, which closed earlier by subduction in the late Paleozoic.

INTRODUCTION

The large Panthalassa oceanic expanse that complemented the Pangea supercontinental lithosphere in late Paleozoic times constituted up to 70% of Earth's surface. Separate-plate status is usually assumed within Panthalassa for the Tethys, Mongol-Okhotsk, and paleo-Pacific oceanic domains (Cogné et al., 2005; van der Meer et al., 2010, 2012), but the complete disappearance through subduction of these domains renders paleogeographic depiction of the extent and boundaries of these plates rather speculative. Be that as it may, the Mongol-Okhotsk oceanic domain is generally thought to have subducted under the northeastern Asia continental margin of Pangea and below Mongolian terranes; paleomagnetic data suggest final closure in the latest Jurassic–earliest Cretaceous (Klimetz, 1987; Zhao et al., 1990; Enkin et al., 1992; Besse et al., 1998; Kravchinsky et al., 2002a, 2002b; Torsvik and Cocks, 2004; Cogné et al., 2005; Metelkin et al., 2007; Şengör and Atayman, 2009; Xiao et al., 2010). This ancient ocean has also been called the Khangai-Khantey Ocean (Şengör and Natal'in, 1996).

The overall trend of the suture zone that resulted from closure of the Mongol-Okhotsk Ocean is oriented WSW-ENE (Fig. 1) and parallels the margins of the neighboring continental elements. These include the Siberian craton to the north, and the combined Amuria and North China blocks to the south. The latter two are generally considered to have amalgamated in early Mesozoic time following the closure of the Solonker, or Intra-Asian Ocean (Xiao et al., 2009, 2010). The orientation of the Mongol-Okhotsk Ocean suture has led most authors to conclude that the suture must have been the result of an approximately orthogonal collision between Amuria and Siberia after a NNW-SSE–directed convergence. Roger et al. (2003), for instance, and

Besse et al. (1998), as well as Kravchinsky et al. (2002a), closed the Mongol-Okhotsk Ocean by sliding Amuria (also labeled Manchurides sensu lato, or, simply, Mongolia in some studies) northward along a N-S sinistral transform zone between the Tarim block and Amuria toward a trench in the north that would ultimately develop into the suture.

The transform-fault proposal is convenient, because it could explain why the suture ends without a trace in the eastern Altaids at about longitude 90°E–105°E (Gilder and Courtillot, 1997). However, no such transform fault that should dissect or border Amuria in the west can be positively identified in this area. Instead, Amuria is characterized by a WSW-ENE structural grain defined by arc, ophiolite, and continental rocks that resulted from a long-lasting Paleozoic subduction-accretion history (e.g., Şengör et al., 1993; Badarch et al., 2002; Buchan et al., 2002; Dijkstra et al., 2006; Windley et al., 2007; Wilhem et al., 2012; Heumann et al., 2012). This structural grain runs parallel to the suture all along its similarly oriented trajectory (Fig. 1).
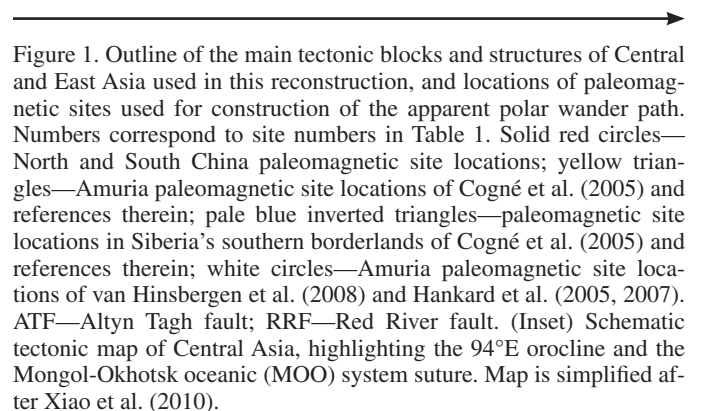
Figure 1. Outline of the main tectonic blocks and structures of Central and East Asia used in this reconstruction, and locations of paleomagnetic sites used for construction of the apparent polar wander path. Numbers correspond to site numbers in Table 1. Solid red circles—North and South China paleomagnetic site locations; yellow triangles—Amuria paleomagnetic site locations of Cogné et al. (2005) and references therein; pale blue inverted triangles—paleomagnetic site locations in Siberia's southern borderlands of Cogné et al. (2005) and references therein; white circles—Amuria paleomagnetic site locations of van Hinsbergen et al. (2008) and Hankard et al. (2005, 2007). ATF—Altyn Tagh fault; RRF—Red River fault. (Inset) Schematic tectonic map of Central Asia, highlighting the 94°E orocline and the Mongol-Okhotsk oceanic (MOO) system suture. Map is simplified after Xiao et al. (2010).
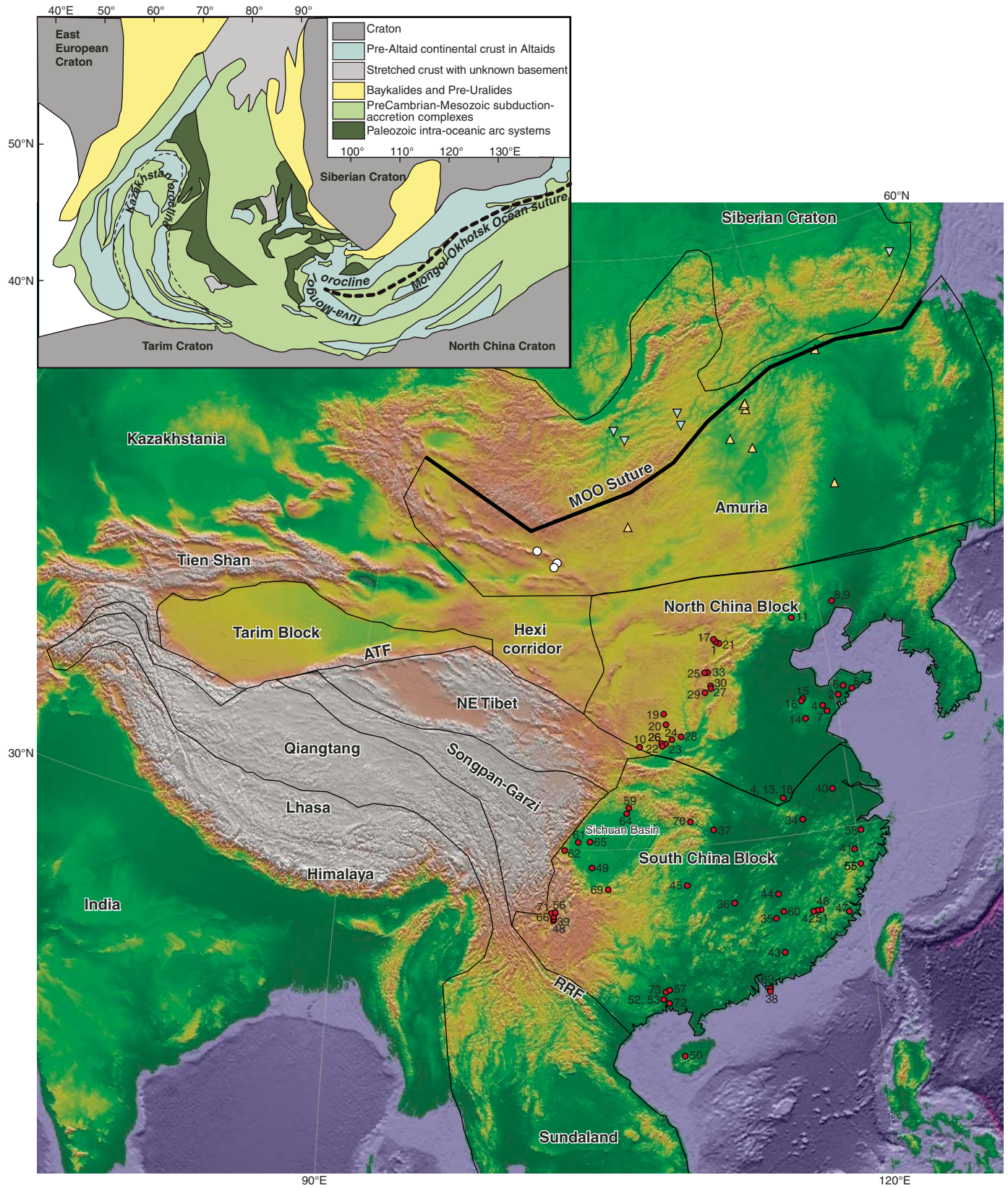
Instead of ending abruptly along a transform fault, the structural grain farther west appears to form a convex-westward, C-shaped, oroclinal curvature at longitude 94°E (Fig. 1; Yakubchuk, 2004; Windley et al., 2007; Xiao et al., 2010; Wilhem et al., 2012). This negates the existence of a Late Jurassic–Early Cretaceous plate boundary between Amuria and Eurasia (i.e., Kazakhstania, Fig. 1) farther west. Moreover, even if the suture turns westward into a crypto-structure, the Mongol-Okhotsk Ocean cannot be called upon to have existed farther to the west of longitude 95°E–100°E, because terrestrial conditions prevailed west and north of the Tarim continental block throughout Mesozoic times (Cocks and Torsvik, 2007; Xiao et al., 2010; Choulet et al., 2011).

In order to establish whether seismic tomographic images may allow us to resolve any deeper slab configurations and, in turn, shed light on the surface kinematics, we return to a previously interpreted and major seismic wave-speed anomaly in the lower 1000 km of the mantle below Siberia. It was previously identified as the slab that subducted as a result of closure of the Mongol-Okhotsk Ocean (Van der Voo et al., 1999), an interpretation that appears to reconcile well with attempts to link lower-mantle structure with reconstructed Mesozoic subduction zones in plate reconstructions on a global scale (van der Meer et al., 2010). The "Mongol-Okhotsk Ocean slab," however, has a N-S orientation, at high angles to the modern trend of the suture zone (Van der Voo et al., 1999).

Thus we have two enigmatic situations surrounding the Mongol-Okhotsk Ocean suture: (1) It appears to be not straightforward to transform a N-S–striking, westward-subducting Mongol-Okhotsk Ocean underneath the Siberian/Amurian margin into an approximately E-W–striking suture, and (2) the suture appears to vanish at ~95°E, without continuation as a plate boundary, which violates plate-tectonic rules, which mandate that all plate boundaries connect to other plate boundaries (Cox and Hart, 1986).

In the following, we will use a compilation of Mesozoic paleomagnetic data from the North China block since Late Permian time to determine rotations and paleolatitudes of this block and compare them to the position of Siberia—since Late Permian time part of Eurasia (Cocks and Torsvik, 2007; Torsvik et al., 2008a)—as defined in the most recent global apparent polar wander path of Torsvik et al. (2012). We then use this paleomagnetic data compilation to construct first-order paleogeographic scenarios, which will illustrate the tectonic development as the Mongol-Okhotsk Ocean was being subducted, and which may provide answers to the earlier-raised questions. Furthermore, we will resort to deep-mantle tomographic imagery and will argue that the orientation of a deep Mongol-Okhotsk Ocean slab underneath Asia today presents an additional line of evidence in support of our model.

GEOLOGICAL CONSTRAINTS ON MONGOL-OKHOTSK OCEAN CLOSURE

Contrary to most suture zones, the Mongol-Okhotsk Ocean suture is not associated with major topography and associated rock exposure, which, in combination with its remote location, has caused geological constraints on its closure history to remain relatively sparse. Rocks exposed within the suture zone consist of folded and thrusted accretionary wedges, which contain relics of more or less complete ophiolite sequences (Natal'in, 1993). Silurian radiolarites overlying dolerites and basalts reveal the oldest demonstrated age for oceanic crust in the Mongol-Okhotsk Ocean (Kurihara et al., 2008). A ca. 325 Ma U/Pb age of leucograbbros in the Adaatsag ophiolite in the east of the suture zone is the oldest direct age of mafic crust of the Mongol-Okhotsk Ocean (Tomurtogoo et al., 2005), and the complete composite ophiolite sequences there indicate that intra-oceanic subduction did occur within the Mongol-Okhotsk Ocean. An intra-oceanic "Onon arc" has been reconstructed to have formed in the Devonian–Mississippian offshore from both the Siberian and Amurian continental margins (Kuzmin and Kravchinsky, 1996; Zorin, 1999), further supporting intra-oceanic subduction within the Mongol-Okhotsk Ocean. Late Permian to Early Jurassic ongoing magmatism in the Onon arc has been interpreted to have occurred in an Andean-style mountain belt after collision of the arc with either the Siberian or Amurian margin (Tomurtogoo et al., 2005). These lines of evidence attest to a complex and long-lived formation and consumption of the Mongol-Okhotsk Ocean from mid-Paleozoic time onward.

Geological constraints for closure during Jurassic time come from several lines of evidence. Volcanic arc rocks have been reported both to the north and to the south of the Mongol-Okhotsk Ocean suture, with ages ranging from Devonian to Jurassic, generally interpreted to reflect long-lasting bivergent subduction below Siberia and Amuria (Bussien et al., 2011; Chen et al., 2011; Donskaya et al., 2012a, 2012b). Decreasing volumes of Upper Jurassic arc magmatic rocks reflect the demise of Mongol-Okhotsk Ocean subduction; Early Cretaceous volcanism on the Siberian side of the suture is devoid of an arc signature but has a within-plate geochemical signature instead and is associated with continental extension (Donskaya et al., 2012b). A ca. 172 Ma U/Pb age of a granitic mylonite close to the Mongol-Okhotsk Ocean suture indicates active mid-Jurassic deformation in the suture zone (Tomurtogoo et al., 2005). Eastward younging trends in magmatism up to mid-Jurassic age at the northeastern end of the suture zone have been used to argue for an eastward closure of the ocean in a scissor-like fashion (Zhao et al., 1990; Zonenshain et al., 1990). Early Cretaceous (ca. 140–100 Ma) enhanced denudation rates constrained by low-temperature thermochronology in the Baikal region are generally interpreted as related to final closure of the Mongol-Okhotsk Ocean (van der Beek et al., 1996; Glorie et al., 2012; Jolivet et al., 2013).

In summary, geological estimates of the age of closure of the Mongol-Okhotsk Ocean rely on interpretations of the geochemistry of magmatic rocks and the tectonic significance of low-temperature thermochronological data; be that as it may, these interpretations suggest that final closure of the Mongol-Okhotsk Ocean occurred sometime in Late Jurassic–Early Cretaceous time.

PALEOMAGNETIC DATA SELECTION AND APPARENT POLAR WANDER PATH CONSTRUCTION

A paleomagnetic analysis of the Mongol-Okhotsk Ocean closure history requires temporally distributed data from both north and south of the suture. An ideal analysis would contrast coeval data from the margins of the Mongol-Okhotsk Ocean suture, but paleomagnetic studies conducted in Amuria have so far been limited, and the structural complexities of this tectonically disturbed area have rendered many available data inscrutable (Cogné et al., 2005). We have thus elected to examine the history of this region primarily from the vantage point of the stable cratons to the north (Siberia) and south (North and South China) of Amuria. According to the union of Siberia and Laurussia in the latest Paleozoic (ca. 251 Ma), we are able to substantially supplement the paleomagnetic record for Siberia through utilization of the global apparent polar wander path of Torsvik et al. (2012). However, because the North and South China blocks remained independent of Eurasia perhaps as late as the earliest Cretaceous, they necessitate a separate and block-specific paleomagnetic data compilation (Figs. 1B, 2, and 3; Table 1).

Due to the paucity of paleomagnetic data from China for the intervals of greatest interest, we have adopted an inclusive approach to data selection: Data sets only required a minimum of three sites or 25 samples, the application of stepwise demagnetization, and some form of vector analysis of the magnetization directions (for lack of data in the Middle-Late Triassic, we relaxed the demagnetization requirement and accepted three results that were only treated by blanket demagnetization; these results [entries 22, 25, 26] are marked by an asterisk in Table 1). As will be discussed later herein, age estimates on sampled sedimentary sections are typically very broad, often owing to poor stratigraphic and geochronologic resolution in massive terrestrial successions; we correspondingly accepted data with age constraints that loosely fit within a geologic period (~50 m.y.). Because many critical poles come from tectonically stable areas (e.g., the Sichuan Basin, Fig. 1), field tests cannot always be applied and so were not essential for inclusion in our compilation; however, data sets that failed a field test were dismissed. The presence of reversals and a lack of resemblance to younger paleomagnetic poles were also not general requirements, as much of the available paleomagnetic data are associated with the long Cretaceous normal superchron and the so-called Cretaceous–Paleogene "standstill."

In order to eliminate uncertainties introduced by the usage of data from peripheral blocks (i.e., poorly established timing of amalgamation and/or restoration parameters), we only accepted data from the North and South China blocks themselves. Specifically, data from separate blocks, such as the Eastern Liaoning-Korean block, which may have rotated with respect to the North China block in the Cenozoic (Uno, 2000; Lin et al., 2003), were excluded. Paleomagnetic results from the Hexi and Gansu corridors (Frost et al., 1995; Yan et al., 2013) revealed local and regional rotations, ruling them out for our purposes, and sug-

gesting that other paleomagnetically studied formations from the same area should also not be used (Chen et al., 2002; Dupont-Nivet et al., 2003, 2008; Liu et al., 2010). We further excluded data from the South China block prior to 170 Ma, when there is some controversy regarding the timing of its collision with the North China block. High- to ultrahigh-pressure metamorphism (ca. 220–200 Ma) followed by exhumation (ca. 200–170 Ma) along the Qinling-Dabieshan suture have been traditionally interpreted as the signature of a Late Triassic collision between the Chinese blocks (Ames et al., 1993; Okay et al., 1993; Eide et al., 1994; Hacker et al., 1998; Li et al., 2000; Yang and Besse, 2001). Paleomagnetic investigations of the collision have conversely concluded that convergence between the blocks continued well into the Middle Jurassic (Yang et al., 1992; Gilder and Courtillot, 1997; Yang and Besse, 2001; Uno and Huang, 2003) or even the Late Jurassic (Yokoyama et al., 2001). It is not our purpose here to explore this discrepancy, but rather to ensure that relative rotations between the North China block and South China block do not introduce artifacts into the paleomagnetic analysis of the Mongol-Okhotsk Ocean closure; we thus conservatively elected to dismiss data from the South China block prior to 170 Ma (Table 1, entries 69–73). Finally, several poles from the south and western margins of the South China block, notably along the Red River fault, are suspected to have been subjected to local vertical-axis rotations, either by tectonic activity associated with the collision of India and the extrusion of Indochina in the Cenozoic, or through regional extension related to circum-Pacific subduction since the Cretaceous (Gilder et al., 1993a; Li et al., 1995, 2005; Liu and Morinaga, 1999; Zhu et al., 2006; Wang and Yang, 2007; Kawamura et al., 2013). Because the recognition of a local vertical-axis rotation requires a comparison against a stable reference—which we have not yet discussed—we provisionally accepted these data into our compilation, to be revisited later herein (bold and underlined in Table 1).

Following the extensive discussion in Torsvik et al. (2012), we corrected all clastic sedimentary paleomagnetic data for an assumed shallow inclination bias of $f = 0.6$ (see also Bilardello et al., 2013), except where a specific correction was calculated in the original study (e.g., Wang and Yang, 2007). At this stage, it became apparent that the Late Jurassic Tiaojishan pole of Pei et al. (2011) is notably discordant ("T" in Fig. 2A). Pei et al. (2011) reported that poor outcrop conditions only permitted structural orientation measurements to be made at two (of 15) sites; considering the measured angle of dip (61°) and the difficulty of determining paleohorizontal in andesitic lavas, we speculate that the resulting pole is anomalous due to poor structural control, and we dismiss it from our analysis.

Our final compilation includes 67 paleomagnetic poles, 32 from the North China block (260–66 Ma) and 35 from the South China block (170–66 Ma). Here, we note that the paleomagnetic data from the Middle Jurassic of the South China block, although badly scattered, are not dissimilar from those of the North China block alone, suggesting that our merger of the two data sets by 170 Ma is reasonable (Fig. 2A). Due to the commonly broad age
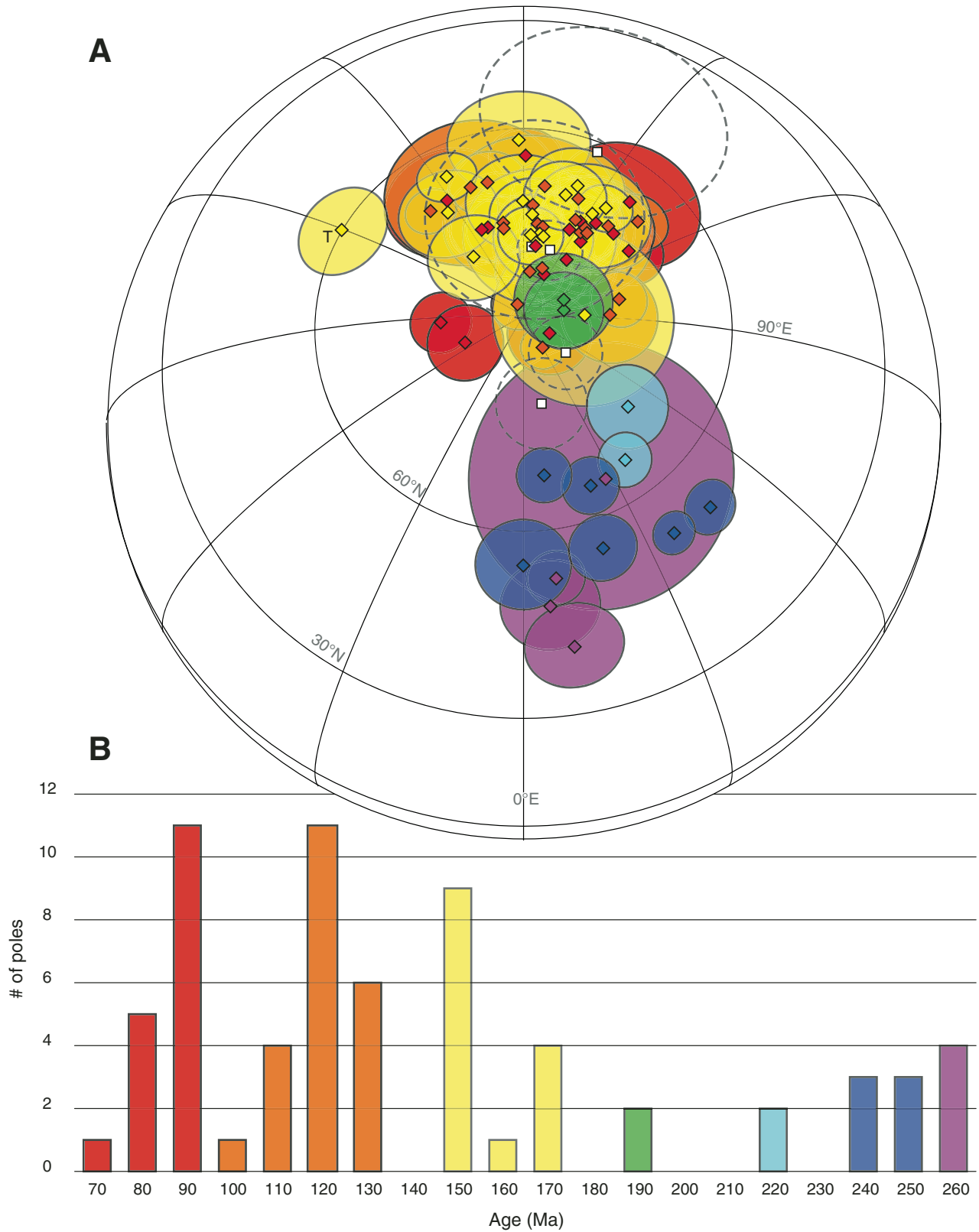
Figure 2. (A) Paleomagnetic poles from the North and South China blocks after correction for inclination shallowing (Table 1). The paleopoles are color-coded according to the scheme displayed in panel B. T—pole 11 of Pei et al. (2011), which has been discarded as discussed in the text. The white squares and associated dashed A95s represent the Early Jurassic poles from the South China block (poles 69–73). (B) Number of paleomagnetic data versus age in 10 m.y. bins.
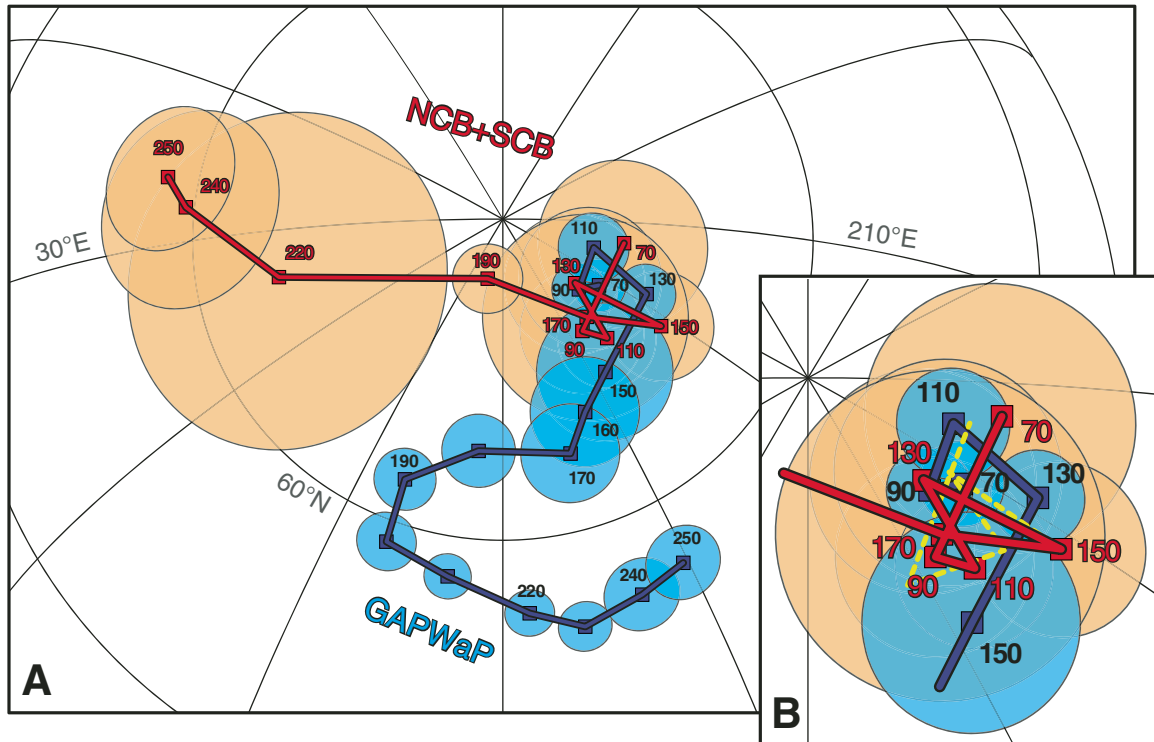
Figure 3. (A) Global apparent polar wander path (GAPWaP) in Eurasia coordinates (from Torsvik et al., 2012) and APWP segments for the North and South China block (NCB and SCB, respectively; data in Table 2). Paths were constructed using 10 m.y. time steps and 20 m.y. moving windows. However, to remove redundant poles (due to data paucity) and for clarity, some poles have been removed from the illustration. The complete data are listed in Table 2. (B) In addition to calculating the apparent polar wander path of North and South China with all available data listed in Table 1, we have also calculated an alternative path segment (150–70 Ma, dashed, yellow) after removing data suspected of having experienced local vertical-axis rotations. It can be seen that this adjustment does not make a significant difference.

assignments as discussed already, the temporal distribution of data appears serrated (Fig. 2B). To mitigate this artifact where possible, we attempted to discriminate between Early (Late) Cretaceous data acquired during the long Cretaceous normal superchron (121–83 Ma; Cande and Kent, 1995; He et al., 2008) from those acquired before (subsequent to) it. To this end, we arbitrarily added 5 m.y. to the assigned age of Early Cretaceous paleomagnetic results with reverse polarity (i.e., the assigned age changes from 123 to 128 Ma) and vice versa for Early Cretaceous data with normal polarity only (age changes from 123 to 118 Ma). Similarly, the assigned age of Late Cretaceous data with reverse (only normal) polarity were adjusted from 83 to 78 Ma (88 Ma).

To compare our assembled paleomagnetic data from the North China block + South China block directly against the "Siberian" data (global apparent polar wander path), we constructed an apparent polar wander path by taking a moving average of the compiled poles at 10 m.y. intervals with a 20 m.y. sliding window (Fig. 3). Because of the noted artifact in the distribution of pole ages, it should be borne in mind that neighboring time steps in our apparent polar wander path are strongly related, and the lurching appearance of the complete path is likely artificial. We

thus prefer to focus on select intervals (as shown in Fig. 3) where the mean is relatively well defined and largely independent. To consider the influence that possibly rotated poles have on our North China block + South China block apparent polar wander path, we have recalculated the path after excluding these poles (bold and underlined in Table 1); the result is minor (Fig. 2) and restricted to the Cretaceous.

PALEOGEOGRAPHIC RECONSTRUCTIONS

We then used the paleomagnetic data compiled into an apparent polar wander path for the North China block in the previous section to build a paleogeographic reconstruction of Triassic–Jurassic Mongol-Okhotsk Ocean closure. The following constraints and assumptions were used. Firstly, the paleolatitude and vertical-axis rotation relative to Earth's magnetic dipole for the North China block were derived from its apparent polar wander path and for Siberia from the global apparent polar wander path of Torsvik et al. (2012) (Table 2). Reconstructions were made with GPlates (Boyden et al., 2011).

The apparent polar wander paths were translated into a paleolatitude graph (Fig. 4) at a reference point on the Mongol-Okhotsk

TABLE 1. SELECTED NORTH AND SOUTH CHINA PALEOMAGNETIC DATA

Site no.	Rock unit	Mean age (Ma)	Slat (°N)	Slong (°E)	N(n)	Dec (°)	Inc (°)	α95 (A95, °)	f	Corr. inc. (°)	Plat (°N)	Plong (°E)	Reference[†]
North China block													
1	Zuoyan Formation limestones, Datong area, Shanxi Province	78	40.1	112.9	4(29)	12.4	63.4	**5.8**	1	63.4	79.7	170.8	a
2	Wangshi Group, Jiaodong Peninsula	88	36.6	120.3	8(59)	1.0	46.5	**5.3**	1	46.5	81.1	294.5	b
3	Cretaceous tuffs and red beds, Anui/Henan Provinces	100	31.9	116.0	10	18.0	50.6	**4.7**	0.6	63.8	70.6	156.7	c
4	Qingshan Group (Lushan & Shidui localities), Jiaodong Peninsula	113	36.2	119.2	8(51)	16.3	58.3	5.2	1	58.3	76.8	192.1	b (recalc.)
5	Weideshan and Haiyang plutons, Jiaodong Peninsula	116	36.8	121.2	20	6.6	59.8	4.6	1	59.8	83.6	172.3	d
6	"Area IV", Qingshan Group, Shandong Province	118	37.0	120.7	11	10.3	54.8	**5.9**	0.6	67.1	75.2	147.7	f
7	Andesites and tuffs, Shandong Province	118	35.9	119.4	5(48)	26.1	55.7	12.2	1	55.7	69.0	200.7	g
8	Basaltic lavas, Zhuanchengzi section, Liaoning Province	121	41.3	121.1	20	353.1	60.1	3.0	1	60.1	84.8	30.2	h
9	Yixian Formation lavas, Liaoning Province	121	41.3	121.0	12	6.7	64.9	6.5	1	64.9	82.7	159.6	i
10	Zhidan Group, Ordos Basin	128	35.1	107.6	10	16.4	50.5	6.8	0.6	63.7	73.9	153.3	j
11	Tiaojishan Formation volcanics, Chengde area	155	40.8	118.1	9(66)	27.1	37.9	**6.8**	1	37.9	59.9	240.3	e
12	Laiyang Formation, Shandong Province	155	35.9	119.4	10	20.6	47.8	7.9	0.6	61.5	72.8	180.3	g
13	Maotangchang and Heishidu Fms., Anui/Henan Provinces	155	31.9	116.0	10	16.7	43.7	**5.9**	0.6	57.9	74.9	175.4	c
14	"Area II," Laiyang Group, Shandong Province	155	35.7	118.0	5(44)	12.3	48.2	**6.9**	0.6	61.8	78.0	166.8	f
15	"Area III," Laiyang Group, Shandong Province	155	36.7	118.0	6(41)	20.5	54.0	**5.7**	0.6	66.4	70.7	162.2	f
16	Santai Formation, Shandong Province	160	36.6	117.9	4(26)	22.3	55.8	6.6	0.6	67.8	68.7	159.1	g
17	Yungang and Datong Fms., Datong area, Shanxi Province	169	40.2	112.8	3(19)	17.9	58.7	**8.3**	0.6	70.0	71.8	148.2	a
18	Zhuji and Zhougongshan Fms., Anui/Henan Provinces	169	31.9	116.0	17	12.4	33.5	**6.4**	0.6	47.8	78.9	218.6	c
19	Middle Jurassic sediments, Yan'an area, Ordos Basin	169	36.7	109.2	6(34)	14.4	45.9	4.5	0.6	59.8	78.1	175.2	k
20	Lower Jurassic sediments, Yan'an area, Ordos Basin	188	36.2	109.3	10	0.5	47.4	6.8	0.6	61.1	84.0	112.9	k
21	Lower Jurassic sandstones, Ordos Basin and Datong area	188	40.0	113.1	15	358.0	50.6	**5.5**	0.6	63.8	84.4	98.6	l
22	Yanchan Group, Ordos Basin, Shanxi Province*	219	35.1	109.0	21	337.4	48.1	**5.8**	0.6	61.7	70.9	49.8	m
23	Upper Triassic sediments, Tongchuan section, Ordos Basin	219	35.2	109.2	11	329.6	43.7	**3.8**	0.6	57.9	65.6	36.1	n
24	Mid-Triassic seds., Hancheng & Tongchuan sections, Ordos Basin	242	35.4	109.6	17	329.5	37.5	**4.0**	0.6	52.0	64.7	22.1	n
25	Zhifang Formation, Ningwu Basin, Shanxi Province*	242	38.6	112.0	20	312.0	43.2	3.1	0.6	57.4	52.8	36.6	o
26	Zhifang Formation, Ordos Basin, Shanxi Province*	242	35.2	109.0	2(25)	311.5	48.8	3.9	0.6	62.3	52.2	46.9	o
27	Liujiagou Formation, Taiyuan, Shanxi Province	250	37.8	112.3	(25)	325.9	22.8	6.6	0.6	35.0	55.1	359.9	p
28	Lower Triassic sediments, Hancheng section, Ordos Basin	250	35.5	110.2	16	335.2	32.5	**3.8**	0.6	46.7	67.7	7.5	q
29	Liujiagou and Ermaying Fms., Shanxi Province	250	37.6	111.9	14	319.8	33.8	**4.8**	0.6	48.1	55.7	19.8	r
30	Shiqianfeng and Upper Shihezi Fms., Shanxi Province	256	37.9	112.3	8(22)	328.3	40.9	18.9	0.6	55.3	64.7	27.4	s
31	Upper Shihezi and Shiqianfeng Formations, Shanxi Province	256	37.8	112.3	12	318.4	21.5	6.9	0.6	33.3	48.8	5.6	t
32	Shiqianfeng & Upper Shihezi Fms., Taiyuan, Shanxi Province	256	37.8	112.3	(89)	321.2	25.3	4.0	0.6	38.2	52.9	7.4	q
33	Shihezi Formation, Jingle Area, Shanxi Province	256	38.6	112.1	2(33)	310.7	20.0	**6.9**	0.6	31.2	42.0	9.5	u
South China block													
34	Wanghudun, Xuannan, Changqiao Fms., near Dabieshan	66	30.7	117.0	7(45)	8.4	47.7	6.4	0.6	61.4	76.4	144.4	f
35	Upper Cretaceous red beds, Ganzhou area, Jiangxi Province	78	25.9	114.9	14	15.6	44.4	**5.2**	1	44.4	76.0	200.7	v
36	Daijiaping Formation, Hengyang basin, Hunan Province	78	26.9	112.6	26	15.6	29.9	**4.7**	0.6	43.8	76.0	204.4	w
37	Paomagang Formation, Yichang area	78	30.7	111.7	26	3.8	23.3	**4.3**	0.6	35.7	78.5	273.4	x
38	**Hong Kong dikes**	80	22.2	114.2	12	21.7	33.4	**8.9**	1	33.4	69.3	211.2	y
39	Xiaobu Formation, Sichuan Province	88	26.6	102.4	3(20)	12.6	46.2	5.3	0.6	60.1	72.3	135.1	z
40	Puko and Yanzijing Fms., Nanjing area	88	32.0	119.0	10	13.7	58.0	**10.3**	0.6	69.4	66.7	140.0	aa
41	Upper Cretaceous sandstones, Zhejiang Province	88	28.8	119.8	19	10.4	45.5	**6.4**	0.6	59.5	75.7	153.6	bb
42	Upper Cretaceous sandstones, Fujian Province	88	26.0	117.0	22	11.5	44.2	**5.8**	0.6	58.3	73.8	150.7	bb
43	Upper Cretaceous sandstones, Guangdong Province	88	24.1	115.2	9(60)	10.7	44.0	**7.7**	0.6	58.1	72.7	144.3	bb
44	**Upper Cretaceous red beds, Jishuia area, Jiangxi Province**	88	27.1	115.1	10	355.7	48.2	**5.8**	1	48.2	85.7	55.3	v
45	Upper Cretaceous red beds, Yuanma Basin, Hunan Province	88	28.0	110.0	17	6.2	50.3	**5.0**	0.6	63.5	72.2	124.4	cc
46	**Shaxian Formation, Fujian Province**	88	26.0	117.4	2(20)	27.1	40.2	**5.0**	0.6	54.6	65.0	179.4	dd
47	Shimaoshan Group volcanics, Fujian Province	88	25.7	119.0	19	4.5	50.2	**3.9**	1	50.2	83.4	154.9	ee
48	Xiaoba Formation, Sichuan Province	93	26.5	102.4	18	8.1	38.8	**7.1**	0.6	53.3	79.9	144.2	ff
49	Guanyin section red beds, Sichuan Province	106	29.1	104.6	13	16.1	33.5	8.3	0.6	47.8	75.9	191.6	gg
50	**Lumuwan Formation, Hainan Island**	112	19.2	109.4	17	10.9	44.1	**4.4**	0.6	58.2	68.1	132.7	hh+ii
51	Hekou Formation, Fujian Province	113	26.0	117.2	5(27)	23.5	33.5	**5.4**	0.6	47.8	69.0	194.0	jj
52	Xinlong Fm., east area, Guangxi Province	118	22.2	108.4	12	10.8	39.1	**9.2**	0.6	53.6	74.8	144.6	kk
53	**Xinlong Fm., west area, Guangxi Province**	118	22.2	108.4	17	358.1	40.7	**4.0**	0.6	55.1	76.5	101.8	kk
54	Lower Cretaceous red beds, Yuanma Basin, Hunan Province	118	28.0	110.0	13	12.0	48.5	**6.6**	0.6	62.0	71.9	139.2	cc

(Continued)

TABLE 1. SELECTED NORTH AND SOUTH CHINA PALEOMAGNETIC DATA (*Continued*)

Site no.	Rock unit	Mean age (Ma)	Slat (°N)	Slong (°E)	N(n)	Dec (°)	Inc (°)	α95 (A95, °)	f	Corr. inc. (°)	Plat (°N)	Plong (°E)	Reference[†]
South China block (continued)													
55	Lower Cretaceous sandstones, Zhejiang Province	118	28.8	120.0	**19**	9.6	47.6	**6.9**	0.6	61.3	74.3	146.9	bb
56	Feitianshan Formation, Sichuan Province	118	26.8	102.5	7(35)	22.1	37.1	**4.3**	0.6	51.6	70.1	171.5	ff
57	**Xinlong Formation, Guangxi Province**	123	22.7	108.7	**8(72)**	355.9	39.1	**6.8**	0.6	53.6	78.0	92.1	dd
58	Chaochuan and Guantuo Fms., Zhejiang Province	128	29.7	120.3	7(62)	13.6	42.7	**5.5**	0.6	57.0	76.2	171.9	g
59	Bailong and Cangxi Fms., Sichuan Basin	128	32.1	106.8	**30**	20.9	26.5	**3.6**	0.6	39.7	69.2	218.9	ll
60	Lower Cretaceous sandstones, Ganzhou & Xinggou Basins, Jiangxi Prov.	128	26.2	115.3	**23**	12.9	38.6	**3.3**	0.6	53.1	76.6	168.6	mm
61	Xinjin section red beds, Sichuan Province	128	30.4	103.8	4(35)	19.2	39.2	12.1	0.6	53.7	73.4	175.6	gg
62	Ya'an red beds, Sichuan Province	128	30.0	103.0	**26**	2.0	34.2	**3.6**	0.6	48.6	88.2	207.8	nn
63	Hong Kong granites	153	22.3	114.2	**12**	11.5	47.8	**10.6**	1	47.8	77.7	169.4	oo
64	Penglaizhen Formation, Sichuan Basin	155	31.8	106.7	(36)	20.0	28.8	**7.0**	0.6	42.5	71.0	213.9	pp
65	Penglaizhen Formation, near Jiangyang, Sichuan Basin	155	30.4	104.5	**24**	25.9	26.7	**4.2**	0.6	40.0	65.7	206.6	qq
66	Xichang-Huili red beds, Sichuan Province	155	26.7	102.4	**20**	17.9	45.6	**3.8**	0.6	59.6	69.8	145.1	rr
67	Xingshan-Zigui section, Hubei Province	155	31.2	110.4	4(49)	33.1	41.1	9.9	0.6	55.5	62.2	181.4	tt
68	Xingshan-Zigui section, Hubei Province	169	31.2	110.4	7(91)	356.5	44.3	12.7	0.6	58.4	81.6	91.5	tt
Early Jurassic poles from South China block (not used in APWP)													
69	*Ziliujing-Suining Fms., Xuyong area, Sichuan Basin*	*183*	*28.0*	*105.5*	*10*	*10.0*	*38.7*	***4.5***	*0.6*	*53.2*	*79.7*	*159.3*	*uu*
70	*Xingshan-Zigui section Hubei Province*	*188*	*31.2*	*110.4*	*9(140)*	*351.7*	*39.6*	*5.1*	*0.6*	*54.0*	*82.3*	*48.5*	*tt*
71	*Xichang-Huili red beds, Sichuan Province*	*188*	*26.8*	*102.3*	*8(34)*	*30.3*	*44.6*	*16.1*	*0.6*	*58.7*	*61.8*	*158.0*	*rr*
72	*Daling Formation, Guangxi Province*	*188*	*22.0*	*108.7*	*4(47)*	*346.8*	*23.5*	*6.3*	*0.6*	*35.9*	*77.5*	*11.5*	*vv*
73	*Wangmen Formation, Guangxi Province*	*188*	*22.6*	*108.5*	*3(31)*	*10.3*	*30.9*	*14.0*	*0.6*	*44.9*	*79.9*	*173.8*	*vv*

Note: Slat/Slong—sampling site latitude/longitude, *N*(*n*)—number of sites (samples) used in calculations, *f*—assumed sedimentary flattening factor, corr. inc—inclination after correction according to *f*, Plat/Plong—latitude/longitude of a paleomagnetic pole calculated after inclination correction where necessary. Bold and underlined entries are poles suspected of having experienced local vertical-axis rotations. Italicized entries were not used in the calculation of the apparent polar wander path (APWP).

*Data that have only been subjected to blanket demagnetization.

[†]References: a—Zheng et al. (1991); b—Huang et al. (2007), recalc.—recalculated from the original reference; c—Gilder and Courtillot (1997); d—Charles et al. (2011); e—Pei et al. (2011); f—Gilder et al. (1999); g—Lin (1984); h—Zhu et al. (2001); i—He et al. (2008); j—Ma et al. (1993); k—Yang et al. (1992); l—Uno and Huang (2003); m—Wu et al. (1990); n—Yang et al. (1991); o—Fang et al. (1988); p—Cheng et al. (1988); q—Embleton et al. (1996); r—Huang et al. (2005); s—Lin et al. (1984); t—McElhinny et al. (1981); u—Zhao and Coe (1989); v—Wang and Yang (2007); w—Sun et al. (2006); x—Narumoto et al. (2006); y—Li et al. (2005); z—Zhu et al. (1988); aa—Kent et al. (1986); bb—Morinaga and Liu (2004); cc—Zhu et al. (2006); dd—Gilder et al. (1993b); ee—Huang et al. (2012); ff—Huang and Opdyke (1992); gg—Enkin et al. (1991b); hh—Liu and Morinaga (1999); ii—Li et al. (1995); jj—Zhai et al. (1992); kk—Kawamura et al. (2013); ll—Sato et al. (2011); mm—Tsuneki et al. (2009); nn—Enkin et al. (1991a); oo—Chan (1991); pp—Yokoyama et al. (1999); qq—Yokoyama et al. (2001); rr—Huang and Opdyke (1991); tt—Wu et al. (1999); uu—Yang and Besse (2001); vv—Gilder et al. (1993a).

TABLE 2. MEAN POLES

Age (Ma)	No. poles	Plat (°)	Plong (°)	A95 (°)	Rdec (°)	Rinc (°)	Rlat (°)
North China block + (South China block after 170 Ma)							
60	1	76.4	144.4	6.4	15.3	74.9	61.7
70	6	78.6	200.0	8.0	18.0	67.2	50.0
80	15	79.1	168.1	5.7	16.4	71.4	56.1
90	13	77.2	155.5	5.8	17.3	73.4	59.2
100	3	76.2	164.9	11.3	20.8	72.5	57.7
110	13	75.3	161.6	4.6	21.9	73.1	58.8
120	20	78.0	162.5	4.1	17.3	72.3	57.5
130	9	81.1	168.0	6.6	13.1	70.9	55.3
150	10	72.3	177.0	5.1	28.9	70.8	55.2
160	14	74.7	174.3	4.7	24.6	71.2	55.8
170	5	78.0	160.7	9.6	17.0	72.5	57.8
180	2	84.2	106.0	3.3	358.9	71.8	56.7
190	2	84.2	106.0	3.3	358.9	71.8	56.7
210	2	68.4	42.1	16.0	324.5	69.6	53.3
220	2	68.4	42.1	16.0	324.5	69.6	53.3
240	6	59.1	23.5	9.6	315.9	61.4	42.5
250	10	56.5	18.0	7.1	315.2	57.9	38.6
Siberia (GAPWaP; Torsvik et al., 2012)							
60	44	78.2	172.6	2.1	18.3	71.0	55.5
70	32	79.2	175.7	2.5	16.9	70.5	54.6
80	25	79.7	177.9	2.9	16.2	70.1	54.2
90	28	80.4	167.2	2.5	14.1	71.2	55.7
100	14	80.8	152.3	3.3	11.1	72.4	57.6
110	21	81.2	193.1	3.3	14.1	68.3	51.5
120	28	79.0	190.1	2.6	17.6	68.6	52.0
130	18	75.0	183.4	2.8	24.3	69.6	53.4
140	9	72.4	187.9	6	28.4	68.6	51.9
150	15	72.9	154.2	6.4	24.6	74.9	61.6
160	19	70.5	143.4	5.1	25.1	77.3	65.8
170	18	67.3	136.4	4.6	27.4	79.5	69.7
180	33	68.3	113.9	3.4	2.4	81.1	72.7
190	46	64.1	98.8	2.9	337.1	82.5	75.2
200	39	57.9	99.3	2.8	318.1	84.9	79.9
210	41	56.1	110.8	2.2	352.5	87.4	84.9
220	35	52.8	124.1	2.3	71.7	86.2	82.3
230	33	50.7	132.1	2.5	83.5	83.6	77.3
240	31	52.2	141.5	3.6	74.7	80.7	71.8
250	34	53.4	149.2	3.6	69.3	78.2	67.3

Note: Apparent polar wander paths for North and South China and Siberia (global apparent polar wander path [GAPWaP] from Torsvik et al., 2012). Both apparent polar wander paths were calculated by a moving average at 10 m.y. intervals with a sliding window of 20 m.y. No. poles—number of constituent poles used to calculate the mean; Plat/Plong—latitude/longitude of the mean paleopole. A95 is the radius of a cone around a mean that contains the true mean direction with 95% probability; it is the same as the α_{95}, with one difference: A95 is based on the mean of virtual geomagnetic poles (VGPs), whereas α_{95} is based on the mean of magnetic directions (declinations and inclinations). Rdec/Rinc/Rlat—declination, inclination, latitude, respectively, calculated from the apparent polar wander paths for a reference point at 51°N, 112°E.

Ocean suture (51°N, 112°E), coinciding with the reference point for Amurian paleomagnetic data of Cogné et al. (2005). The paleolatitude curves of the North China block and Siberia straightforwardly show that these domains have converged gradually since Permian time, and overlapping paleolatitudes since ca. 140 Ma confirm earlier inferences that paleomagnetic constraints suggest a latest Jurassic–earliest Cretaceous closure age of the Mongol-Okhotsk Ocean (Enkin et al., 1992; Xu et al., 1997; Halim et al., 1998; Kravchinsky et al., 2002b; Hankard et al., 2007; Metelkin et al., 2007; van Hinsbergen et al., 2008). The paleolatitudes of the North China block suggest a significantly more northerly position than those from Amuria presented by Cogné et al. (2005), but since it is not feasible that Amuria had a more southerly position than the North China block, we will assume that both blocks moved paleolatitudinally in tandem in the Triassic–Jurassic for the chosen reference location. By way of provisional explanation for the mismatched Amurian results, we speculate that several results may have had problematic paleo-horizontal control, as well as too few independent geomagnetic field directions to average out secular variation. It must also be
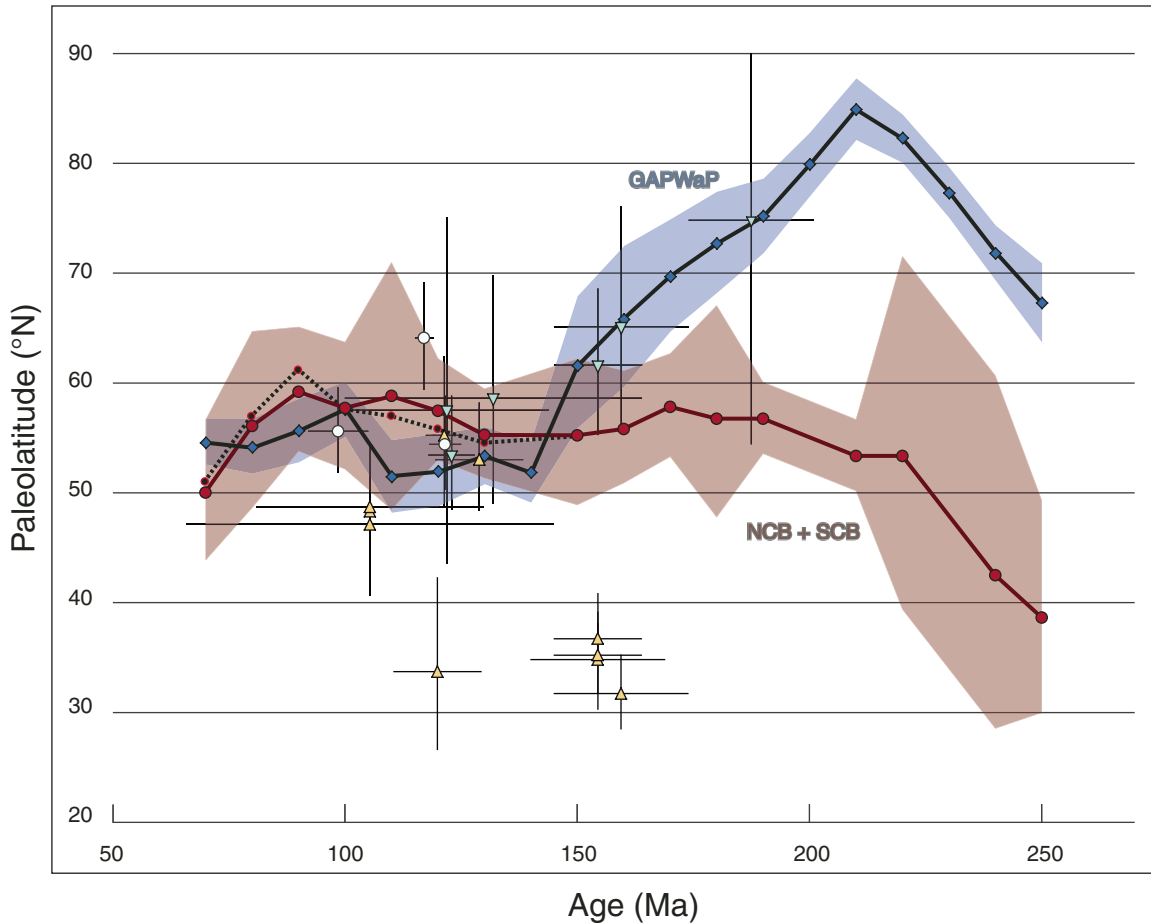
Figure 4. Paleolatitude versus age of reference point 51°N, 112°E according to various paleomagnetic data: 1—North and South China apparent polar wander path (solid red circles with light purple envelope of error), 2—alternative North and South China apparent polar wander path with suspected rotated poles removed (red-outlined circles and dashed black line), 3—Siberian global apparent polar wander path of Torsvik et al. (2012; solid blue diamonds with light blue envelope of error), 4—data of Cogné et al. (2005) from Amuria (yellow triangles), 5—data of Cogné et al. (2005) from Siberia (pale blue inverted triangles), 6—data of van Hinsbergen et al. (2008) and Hankard et al. (2005, 2007) from Amuria (white circles). GAPWaP—global apparent polar wander path; NCB and SCB—North and South China block, respectively.

noted that (uncorrected) inclination shallowing is unlikely to be a factor in this enigma, given the igneous lithologies involved.

Yakubchuk (2004, 2008), Lehmann et al. (2010), and Xiao et al. (2010) noted that the Mongol-Okhotsk Ocean suture appears to end in a tight orocline around 94°E (Fig. 1), termed the "Tuva-Mongol" orocline by Xiao et al. (2010), and suggested that the closure of the Mongol-Okhotsk Ocean was associated with opposing rotations of Siberia and Amuria from an originally approximately N-S–striking, westward-dipping subduction zone to the modern ENE-WSW–trending suture. A noteworthy observation is that these authors suggested closure of the Mongol-Okhotsk orocline in Permian–Triassic rather than latest Jurassic time, which is in disagreement with the available paleomagnetic data, as can be seen in Figures 3 and 4. We model Amuria as the southern limb of an orocline, while it rotated counterclockwise relative to Siberia. Paleomagnetic data from Amuria are

all strongly locally and variably rotated and cannot constrain Amuria's wholesale rotation (Cogné et al., 1995). To determine the rate of rotation of Amuria, we therefore used the North China block's paleomagnetic data as proxy for those of Amuria.

Paleomagnetic data cannot constrain paleolongitude, and we have no independent source of information, such as kimberlites or large igneous provinces (e.g., Torsvik et al., 2008b, 2010), with which to constrain the paleolongitude of the North China block in the Triassic and Jurassic. The paleolongitude of the North China block relative to Siberia is therefore unconstrained. Our apparent polar wander path indicates that the North China block underwent a Jurassic counterclockwise rotation, approximately of the magnitude that would be expected for the combined Amuria–North China block during oroclinal closure of the Mongol-Okhotsk Ocean. We will return to this subject in the analysis section; first, we will test the oroclinal closure scenario

by assessing whether its predictions are consistent with seismic tomographic constraints from the Mongol-Okhotsk Ocean slab.

TOMOGRAPHIC IMAGING OF THE MONGOL-OKHOTSK OCEAN SLAB IN THE DEEP MANTLE AND CORRELATION WITH THE SURFACE PLATE MOTIONS

The oroclinal closure scenario of the Mongol-Okhotsk Ocean predicts that an originally westward-dipping subduction zone was oroclinally bent, leading to both a northward-dipping subduction zone below Siberia, and a southward-dipping subduction zone below Amuria. Opposite senses of rotation (Siberia, clockwise, ~45°; North China block + Amuria, counterclockwise, ~90°) are characteristic of oroclinal bending and are documented by the paleomagnetic results. The latest Jurassic to earliest Cretaceous closure would hence have been associated with a soft docking of Amuria and Siberia. Because neither block was connected through a passive margin with a slab, no continental lithosphere could have been dragged below the opposite continental domain. Instead, the originally southwestward-dipping slab was gradually deformed into two oppositely dipping slabs with ultimately two nearly parallel, approximately E-W–striking trenches. This may explain the absence of a major Himalayan-style fold-and-thrust belt along the Mongol-Okhotsk Ocean suture, and it predicts that the orientation of the Mongol-Okhotsk slab changes with depth.

A tomographic study (Bijwaard et al., 1998) revealed two slab-like positive (i.e., faster) seismic wave velocity anomalies below Siberia. One is clearly connected to present-day subduction underneath Kamchatka, the Kuriles, and Japan, whereas the other, in a more westerly location, is prominent in the deeper mantle, reaching all the way to the core-mantle boundary, where it appears to join a large positive-anomaly mass that has been called a "graveyard of slabs" (Wysession, 1996). The more westerly anomaly was taken to represent an ancient subducted slab, interpreted by Van der Voo et al. (1999) as a remnant of the subducted Mongol-Okhotsk oceanic lithosphere.

To compare our reconstructions to the location and orientation of the seismic tomographic anomaly interpreted by Van der Voo et al. (1999) as the Mongol-Okhotsk Ocean slab, we need to place our paleomagnetism-based reconstruction in a mantle reference frame. To this end, we determined the Euler rotations of the modeled motions of the North China block plus Amuria relative to Siberia. Because we aim to compare surface reconstructions based on paleomagnetic data to mantle structure, we have also to correct the paleomagnetic/mantle reference frame for true polar wander: episodes during which the lithosphere and mantle as a whole (including slabs) rotated relative to the core (and thereby relative to the spin axis; Steinberger and Torsvik, 2008). To this end, we used the true polar wander–corrected reference frame of Torsvik et al. (2012). We then adjusted the plate configuration in paleolongitude by positioning the East China slab (van der Meer et al., 2010, 2012) beneath the eastern margin of the China blocks. Longitude corrections (Tors-

vik et al., 2012) were done prior to the true polar wander correction and then checked in the true polar wander–corrected frame, and repeated until we attained a reasonable fit. For each time interval, we assumed vertical slab sinking at a rate of 12 ± 3 mm/yr (van der Meer et al., 2010).

This procedure results in reconstructed positions of the Mongol-Okhotsk Ocean subduction zone at 140, 160, 180, 200, and 220 Ma (Fig. 5), which we compare with seismic tomographic images at 1690, 1930, 2170, and 2410 km depth (Fig. 6). We note that the orientation of the whole Mongol-Okhotsk Ocean slab is somewhat sinuous, but this may actually correspond to a curved (convex westward) Mongol-Okhotsk Ocean trench on the ocean side of Siberia, Amuria, and North China. The overall pattern of the deeper anomalies attributed to Mongol-Okhotsk Ocean subduction (e.g., at 2410 km, ca. 200 Ma) shows a NNW-SSE trend changing northward to NNE-SSW. This curved set of anomalies (Fig. 6) suggests that earliest Jurassic–Late Triassic subduction occurred in a mildly curved trench. Above it, as described by Van der Voo et al. (1999, p. 247): "At 1,500 [to 1900] km depth, the anomalies form a 'hook,' running first west-northwestwards from Mongolia and then northwards towards the Siberian Arctic coast. At depths of 1,900–2,300 km, the anomalies are gradually more displaced to the west, and display an overall open 'Z'-shaped feature at 2,300 km." We conclude from this description that there is a good congruence with the projected surficial traces of the ancient trenches, which are moderately curved in the 180–200 Ma reconstructions and more tightly curved in the 140–160 Ma reconstructions (Figs. 5 and 6).

Finally, we note that uncertainties in (1) the apparent polar wander path of the North China block and the global apparent polar wander path (typically ~5°); (2) the true polar wander correction (typically a few degrees); (3) the slab-fitting correction (at least ~5°); (4) the likelihood that internal deformation of the tectonic units is insufficiently portrayed in Figure 5; and (5) the validity of the assumption that slabs sink vertically, all may have caused minor departures from perfectly matching features in the comparisons of tomographic images and surface paleogeographic continental configurations. However, our paleogeographic model is consistent with the available kinematic and tomographic data for the region. The large-scale oroclinal bending of the crust above a disappearing ocean is reminiscent of similarly tightening oroclines in Kazakhstan and Variscan Europe, which closed earlier, by subduction in the late Paleozoic (Abrajevitch et al., 2008; Shaw et al., 2012).

We recognize that outside the domain of interest, i.e., around Tarim, Junggar, the Kazakhstan orocline, the Tibetan terranes, and Indochina, various complications may arise from mismatching paleomagnetic and paleogeographic constraints related to this study. It is hoped that future work will provide resolution.

CONCLUSIONS

The suture between Siberia and Amuria (Mongolia) is thought to have formed when the Mongol-Okhotsk Ocean
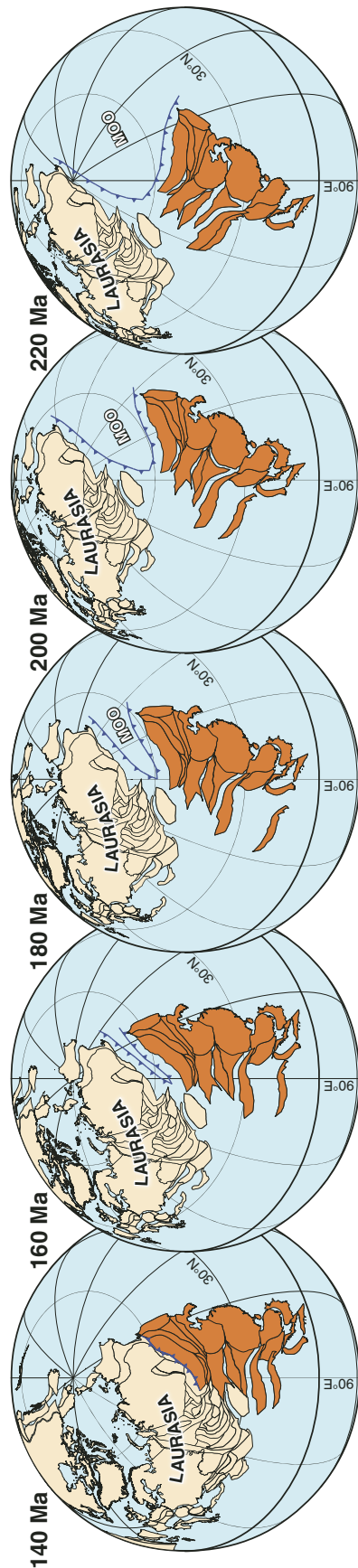
Figure 5. Plate reconstructions shown in a paleomagnetic reference frame, using the apparent polar wander path of the North China block (NCB), as constructed in this paper for the combined North China block and Amuria block (Figs. 2 and 3), and the global apparent polar wander path of Torsvik et al. (2012) for Siberia. Block definitions are given in Figure 1. The South China block (SCB) is drawn as welded to the North China block after 220 Ma (following, e.g., Hacker et al., 2006), but only post–170 Ma paleomagnetic data from the South China block were used for the combined North China block and South China block in this paper (see text). Meridians are in 30° intervals; paleolongitude is based on Africa being stably located in longitude, albeit with a correction of 10° based on the mantle reference frame (see text). MOO—Mongol-Okhotsk Ocean.

subducted completely; the suture strikes WSW-ENE and is identified only to the east of the 100°E meridian. This orientation has been influential in the various proposed models of ocean closure in which Siberia and Amuria approached each other orthogonally (i.e., SSE-NNW) in Late Jurassic–earliest Cretaceous times. This, however, creates the enigma that the suture simply ends without any connection to other ancient plate boundaries.

The enigma is compounded by the tomographic images of the Mongol-Okhotsk Ocean lithospheric slab, which completely detached long ago, i.e., in the (Late?) Cretaceous or earlier, and has been sinking in the deeper lower mantle toward the core-mantle boundary. The lower part of this slab appears to strike N-S, clearly at right angles to the surface suture orientation, albeit with some sinuosity.

We propose a solution to this conundrum by invoking a closure mechanism of the Mongol-Okhotsk Ocean that at first involves southwestward subduction in an increasingly curved trench, followed by a gradual scissors-like collision between Siberia and the combined Amuria–North China block, rotating toward each other and deforming the suture into an oroclinal structure with antiparallel E-W limbs. Zhao et al. (1990) first proposed such a closure mechanism, albeit with an earlier, Permian, age. In support of this model, the tomographic images of the Mongol-Okhotsk Ocean slab are characterized by a generalized N-S trend at depths of ~2170–2400 km, in agreement with the trench orientation. At depths of ~1700–1900 km, on the other hand, the slab shows a hook, with a shape like the letter C. Following the age-depth relationship for sinking lithospheric slabs, as proposed by van der Meer et al. (2010), this would correspond to ages of ca. 160 Ma and 180 Ma, respectively. At shallower depths, less than ~1500 km, corresponding to an age younger than earliest Cretaceous (<140 Ma), the slab's contours become unclear (Van der Voo et al., 1999). This reflects the situation after closure of the Mongol-Okhotsk Ocean between Siberia and the combined Amuria–North China block.

ACKNOWLEDGMENTS

Figure 6. Comparison between reconstructions of the Mongol-Okhotsk Ocean–bordering continental blocks and the seismic tomographic images (UU-P07 model; Amaru, 2007; van der Meer et al., 2010) of the Mongol-Okhotsk Ocean (MOO) slab previously identified by Van der Voo et al. (1999). The age of subduction of the slabs was calculated using the ~12 mm/yr average slab sinking rate following van der Meer et al. (2010). Reconstructions are based on a true polar wander–corrected paleomagnetic frame (Torsvik et al., 2012), albeit fine-tuned in longitude, as explained in the text. EC—East China; Eq.—equator.

REFERENCES CITED

Abrajevitch, A., Van der Voo, R., Bazhenov, M.L., Levashova, N.M., and McCausland, P.J.A., 2008, The role of the Kazakhstan orocline in the late Paleozoic amalgamation of Eurasia: Tectonophysics, v. 455, p. 61–76, doi:10.1016/j.tecto.2008.05.006.

Amaru, M.L., 2007, Global travel time tomography with 3-D reference models: Geologica Ultraiectina, v. 274, 174 p.

Ames, L., Tilton, G.R., and Zhou, G., 1993, Timing of collision of the Sino-Korean and Yangtse cratons: U-Pb zircon dating of coesite-bearing eclogites: Geology, v. 21, p. 339–342, doi:10.1130/0091-7613(1993)021<0339:TOCOTS>2.3.CO;2.

Badarch, G., Cunningham, W.D., and Windley, B.F., 2002, A new terrane subdivision for Mongolia: Implications for the Phanerozoic crustal growth of Central Asia: Journal of Asian Earth Sciences, v. 21, p. 87–110, doi:10.1016/S1367-9120(02)00017-2.

Besse, J., Torcq, F., Gallet, Y., Ricou, L.E., Krystyn, L., and Saidi, A., 1998, Late Permian to Late Triassic palaeomagnetic data from Iran: Constraints on the migration of the Iranian block through the Tethyan Ocean and initial destruction of Pangaea: Geophysical Journal International, v. 135, p. 77–92, doi:10.1046/j.1365-246X.1998.00603.x.

Bijwaard, H., Spakman, W., and Engdahl, E.R., 1998, Closing the gap between regional and global travel time tomography: Journal of Geophysical Research, v. 103, p. 30,055–30,078, doi:10.1029/98JB02467.

Bilardello, D., Jezek, J., and Gilder, S.A., 2013, Role of spherical particles on magnetic field recording in sediments: Experimental and numerical results: Physics of the Earth and Planetary Interiors, v. 214, p. 1–13, doi:10.1016/j.pepi.2012.10.014.

Boyden, J.R., Müller, R.D., Gurnis, M., Torsvik, T.H., Clark, J., Turner, M., Ivey-Law, H., Watson, R., and Cannon, J., 2011, Next-generation plate-tectonic reconstructions using GPlates, *in* Keller, R., and Baru, C., eds., Geoinformatics: Cambridge, UK, Cambridge University Press, p. 95–114, doi:10.1017/CBO9780511976308.008.

Buchan, C., Pfänder, J., Kröner, A., Brewer, T.S., Tomurtogoo, O., Tomurhuu, D., Cunningham, W.D., and Windley, B.F., 2002, Timing of accretion and collisional deformation in the Central Asian orogenic belt: Implications of granite geochronology in the Bayankhongor ophiolite zone: Chemical Geology, v. 192, p. 23–45, doi:10.1016/S0009-2541(02)00138-9.

Bussien, D., Gombojav, N., Winkler, W., and von Quadt, A., 2011, The Mongol-Okhotsk belt in Mongolia—An appraisal of the geodynamic development by the study of sandstone provenance and detrital zircons: Tectonophysics, v. 510, p. 132–150, doi:10.1016/j.tecto.2011.06.024.

Cande, S.C., and Kent, D.V., 1995, Revised calibration of the geomagnetic polarity timescale for the Late Cretaceous and Cenozoic: Journal of Geophysical Research, v. 100, p. 6093–6095, doi:10.1029/94JB03098.

Chan, L.S., 1991, Paleomagnetism of late Mesozoic granitic intrusions in Hong Kong: Implications for Upper Cretaceous reference pole of South China: Journal of Geophysical Research, v. 96, p. 327–335, doi:10.1029/90JB01967.

Charles, N., Chen, Y., Augier, R., Gumiaux, C., Lin, W., Faure, M., Monié, P., Choulet, F., Wu, F., Zhu, R., and Wang, Q., 2011, Palaeomagnetic constraints from granodioritic plutons (Jiaodong Peninsula): New insights on late Mesozoic continental extension in eastern Asia: Physics of the Earth and Planetary Interiors, v. 187, p. 276–291, doi:10.1016/j.pepi.2011.05.006.

Chen, Y., Gilder, S., Halim, N., Cogné, J.-P., and Courtillot, V., 2002, New paleomagnetic constraints on Central Asian kinematics: Displacement along the Altyn Tagh fault and rotation of the Qaidam Basin: Tectonics, v. 21, p. 1042, doi:10.1029/2001TC901030.

Chen, Z., Zhang, L.-C., Wan, B., Wu, H., and Cleven, N., 2011, Geochronology and geochemistry of the Wunugetushan porphyry Cu-Mo deposit in NE China, and their geological significance: Ore Geology Reviews, v. 43, p. 92–105, doi:10.1016/j.oregeorev.2011.08.007.

Cheng, G., Bai, Y., and Sun, Y., 1988, Paleomagnetic study on the tectonic evolution of the Ordos block, North China: Seismology and Geology, v. 10, p. 81–87 [in Chinese].

Choulet, F., Chen, Y., Wang, B., Faure, M., Cluzel, D., Charvet, J., Lin, W., and Xu, B., 2011, Late Paleozoic paleogeographic reconstruction of western Central Asia based upon paleomagnetic data and its geodynamic implications: Journal of Asian Earth Sciences, v. 42, p. 867–884, doi:10.1016/j.jseaes.2010.07.011.

Cocks, L.R.M., and Torsvik, T.H., 2007, Siberia, the wandering northern terrane, and its changing geography through the Palaeozoic: Earth-Science Reviews, v. 82, p. 29–74, doi:10.1016/j.earscirev.2007.02.001.

Cogné, J.-P., Chen, Y., Courtillot, V., Rocher, F., Wang, G., Bai, M., and You, H., 1995, A paleomagnetic study of Mesozoic sediments from the Junggar and Turfan basins, northwestern China: Earth and Planetary Science Letters, v. 133, p. 353–366, doi:10.1016/0012-821X(95)00083-O.

Cogné, J.-P., Kravchinsky, V.A., Halim, N., and Hankard, F., 2005, Late Jurassic–Early Cretaceous closure of the Mongol Okhotsk Ocean demonstrated by new Mesozoic palaeomagnetic results from the Trans-Baikal area (SE Siberia): Geophysical Journal International, v. 163, p. 813–832, doi:10.1111/j.1365-246X.2005.02782.x.

Cox, A., and Hart, R.B., 1986, Plate Tectonics: How It Works: Palo Alto, Blackwell Scientific Publications, 392 p.

Dijkstra, A.H., Brouwer, F.M., Cunningham, W.D., Buchan, C., Badarch, G., and Mason, P.R.D., 2006, Late Neoproterozoic proto-arc ocean crust in the Dariv Range, western Mongolia: A supra-subduction zone endmember ophiolite: Journal of the Geological Society of London, v. 163, p. 363–373, doi:10.1144/0016-764904-156.

Donskaya, T.V., Gladkochub, D.P., Mazukabzov, A.M., De Waele, B., and Presnyakov, S.L., 2012a, The Late Triassic Kataev volcanoplutonic association in western Transbaikalia, a fragment of the active continental margin of the Mongol-Okhotsk Ocean: Russian Geology and Geophysics, v. 53, p. 22–36, doi:10.1016/j.rgg.2011.12.002.

Donskaya, T.V., Gladkochub, D.P., Mazukabzov, A.M., and Ivanov, A.V., 2012b, Late Paleozoic–Mesozoic subduction-related magmatism at the southern margin of the Siberian continent and the 150 million-year history of the Mongol-Okhotsk Ocean: Journal of Asian Earth Sciences, v. 62, p. 79–97, doi:10.1016/ j.jseaes.2012.07.023.

Dupont-Nivet, G., Butler, R.F., Yin, A., and Chen, X.H., 2003, Paleomagnetism indicates no Neogene vertical axis rotations of the northeastern Tibetan Plateau: Journal of Geophysical Research, v. 108, no. B8, p. 2386, doi:10.1029/2003JB002399.

Dupont-Nivet, G., Dai, S., Fang, X., Krijgsman, W., Erens, V., Reitsma, M., and Langereis, C.G., 2008, Timing and distribution of tectonic rotations in the northeastern Tibetan Plateau, *in* Burchfiel, B.C., and Wang, E., eds., Investigations into the Tectonics of the Tibetan Plateau: Geological Society of America Special Paper 444, p. 73–87.

Eide, E.A., McWilliams, M., and Liou, J.G., 1994, ^{40}Ar/^{39}Ar geochronology and exhumation of high-pressure to ultrahigh-pressure metamorphic rocks in east-central China: Geology, v. 22, p. 601–604.

Embleton, B.J.J., McElhinny, M.W., Ma, X., Zhang, Z., and Li, Z.X., 1996, Permo-Triassic magnetostratigraphy in China: The type section near Taiyuan, Shanxi Province, North China: Geophysical Journal International, v. 126, p. 382–388, doi:10.1111/j.1365-246X.1996.tb05298.x.

Enkin, R.J., Chen, Y., Courtillot, V., Besse, J., Xing, L., Zhang, Z., Zhuang, Z., and Zhang, J., 1991a, A Cretaceous pole from South China, and the Mesozoic hairpin turn of the Eurasian apparent polar wander path: Journal of Geophysical Research, v. 96, p. 4007–4027, doi:10.1029/90JB01904.

Enkin, R.J., Courtillot, V., Xing, L., Zhang, Z., Zhuang, Z., and Zhang, J., 1991b, The stationary Cretaceous paleomagnetic pole of Sichuan (South China block): Tectonics, v. 10, p. 547–559, doi:10.1029/90TC02554.

Enkin, R.J., Yang, Z., Chen, Y., and Courtillot, V., 1992, Paleomagnetic constraints on the geodynamic history of the major blocks of China from the Permian to the present: Journal of Geophysical Research, v. 97, p. 13,953–13,989.

Fang, D., Guo, Y., Wang, Z., Tan, X., Fan, S., Yuan, Y., Tang, X., and Wang, B., 1988, Tectonic implications of Triassic and Jurassic paleomagnetic results from Ningwu Basin, Shanxi Province: Kexue Tongbao, v. 2, p. 133–135 [in Chinese].

Frost, G.M., Coe, R.S., Meng, Z.F., Peng, Z.L., Chen, Y., Courtillot, V., Peltzer, G., Tapponnier, P., and Avouac, J.P., 1995, Preliminary Early Cretaceous paleomagnetic results from the Gansu corridor, China: Earth and Planetary Science Letters, v. 129, p. 217–232, doi:10.1016/0012-821X(94)00244-S.

Gilder, S., and Courtillot, V., 1997, Timing of the North-South China collision from new middle to late Mesozoic paleomagnetic data from the North China block: Journal of Geophysical Research, v. 102, p. 17,713–17,727, doi:10.1029/97JB01201.

Gilder, S., Zhao, X., Coe, R.S., Wu, H., and Kuang, G., 1993a, Discordance of Jurassic paleomagnetic data from South China and their tectonic implications: Earth and Planetary Science Letters, v. 119, p. 259–269, doi:10.1016/0012-821X(93)90137-X.

Gilder, S.A., Coe, R.S., Wu, H., Kuang, G., Zhao, X., Wu, Q., and Tang, X., 1993b, Cretaceous and Tertiary paleomagnetic results from southeast China and their tectonic implications: Earth and Planetary Science Letters, v. 117, p. 637–652, doi:10.1016/0012-821X(93)90108-L.

Gilder, S.A., Leloup, P.H., Courtillot, V., Chen, Y., Coe, R.S., Zhao, X., Xiao, W.J., Halim, N., Cogné, J.-P., and Zhu, R., 1999, Tectonic evolution of the Tancheng-Lujiang (Tan-Lu) fault via Middle Triassic to early Cenozoic paleomagnetic data: Journal of Geophysical Research, v. 104, p. 15,365–15,390, doi:10.1029/1999JB900123.

Glorie, S., De Grave, J., Buslov, M.M., Zhimulev, F.I., Elburg, M.A., and Van den Haute, P., 2012, Structural control on Meso-Cenozoic tectonic reactivation and denudation in the Siberian Altai: Insights from multi-method thermochronometry: Tectonophysics, v. 544–545, p. 75–92, doi:10.1016/j.tecto.2012.03.035.

Hacker, B.R., Ratschbacher, L., Webb, L.E., Ireland, T.R., Walker, D.J., and Dong, S., 1998, U-Pb zircon ages constrain the architecture of the ultrahigh-pressure Qinling-Dabie orogen, China: Earth and Planetary Science Letters, v. 161, p. 215–230, doi:10.1016/S0012-821X(98)00152-6.

Hacker, B.R., Wallis, S.R., Ratschbacher, L., Grove, M., and Gehrels, G.E., 2006, High-temperature geochronology constraints on the tectonic history and architecture of the ultrahigh-pressure Dabie-Sulu orogen: Tectonics, v. 25, p. TC5006, doi:10.1029/2005TC001937.

Halim, N., Kravchinsky, V., Gilder, S., Cogné, J.-P., Alexyutin, M., Sorokin, A., Courtillot, V., and Chen, Y., 1998, A palaeomagnetic study from the Mongol-Okhotsk region: Rotated Early Cretaceous volcanics and remagnetized Mesozoic sediments: Earth and Planetary Science Letters, v. 159, p. 133–145, doi:10.1016/S0012-821X(98)00072-7.

Hankard, F., Cogné, J.-P., and Kravchinsky, V., 2005, A new Late Cretaceous paleomagnetic pole for the west of Amuria block (Khurmen Uul, Mongolia): Earth and Planetary Science Letters, v. 236, p. 359–373, doi:10.1016/j.epsl.2005.05.033.

Hankard, F., Cogné, J.P., Quidelleur, X., Bayasgalan, A., and Lkhagvadorj, P., 2007, Paleomagnetism and K-Ar dating of Cretaceous basalts from Mongolia: Geophysical Journal International, v. 169, p. 898–908, doi:10.1111/j.1365-246X.2007.03292.x.

He, H., Pan, Y., Tauxe, L., Qin, H., and Zhu, R., 2008, Toward age determination of the M0r (Barremian–Aptian boundary) of the Early Cretaceous: Physics of the Earth and Planetary Interiors, v. 169, p. 41–48, doi:10.1016/j.pepi.2008.07.014.

Heumann, M.J., Johnson, C.L., Webb, L.E., Taylor, J.P., Jalbaa, U., and Minjin, C., 2012, Paleogeographic reconstruction of a late Paleozoic arc collision zone, southern Mongolia: Geological Society of America Bulletin, v. 124, p. 1514–1534, doi:10.1130/B30510.1.

Huang, B., Shi, R., Wang, Y., and Zhu, R., 2005, Palaeomagnetic investigation on Early–Middle Triassic sediments of the North China block: A new Early Triassic palaeopole and its tectonic implications: Geophysical Journal International, v. 160, p. 101–113, doi:10.1111/j.1365-246X.2005.02496.x.

Huang, B., Piper, D.J.W., Zhang, C., Li, Z., and Zhu, R., 2007, Paleomagnetism of Cretaceous rocks in the Jiaodong Peninsula, eastern China: Insight into block rotations and neotectonic deformation in eastern Asia: Journal of Geophysical Research, v. 112, p. B03106, doi:10.1029/2006JB004462.

Huang, K., and Opdyke, N.D., 1991, Paleomagnetism of Jurassic rocks from southwestern Sichuan and the timing of the closure of the Qinling suture: Tectonophysics, v. 200, p. 299–316, doi:10.1016/0040-1951(91)90021-J.

Huang, K., and Opdyke, N.D., 1992, Paleomagnetism of Cretaceous to Lower Tertiary rocks from southwestern Sichuan: A revisit: Earth and Planetary Science Letters, v. 112, p. 29–40, doi:10.1016/0012-821X(92)90004-F.

Huang, K., and Opdyke, N.D., 1993, Errata: Tectonophysics, v. 219, p. 355, doi:10.1016/0040-1951(93)90179-N.

Huang, S., Pan, Y., and Zhu, R., 2012, Paleomagnetism of the Late Cretaceous volcanic rocks of the Shimaoshan Group in Yongtai County, Fujian Province: Science: China Earth Sciences, v. 56, p. 22–30, doi:10.1007/s11430-012-4519-8.

Jolivet, M., Arzhannikov, S., Arzhannikova, A., Chauvet, A., Vassallo, R., and Braucher, R., 2013, Geomorphic Mesozoic and Cenozoic evolution in the Oka-Jombolok region (East Sayan ranges, Siberia): Journal of Asian Earth Sciences, v. 62, p. 117–133, doi:10.1016/j.jseaes.2011.09.017.

Kawamura, T., Hirota, M., Aoki, H., Morinaga, H., Liu, Y., Ahn, H.-S., Zaman, H., Yokoyama, M., and Otofuji, Y.-I., 2013, Tectonic deformation in the southern part of South China block: Paleomagnetic study of the Early Cretaceous Xinlong Formation from Shangsi foredeep depozone in the Guangxi Province: Journal of Geodynamics, v. 64, p. 40–53, doi:10.1016/j.jog.2012.10.005.

Kent, D.V., Xu, G., Huang, K., Zhang, W.Y., and Opdyke, N.D., 1986, Paleomagnetism of Upper Cretaceous rocks from South China: Earth and Planetary Science Letters, v. 79, p. 179–184, doi:10.1016/0012-821X(86)90051-8.

Klimetz, M.P., 1987, The Mesozoic tectonostratigraphic terranes and accretionary heritage of south-eastern mainland Asia, *in* Leitch, E.C., and Scheibner, E., eds., Terrane Accretion and Orogenic Belts: American Geophysical Union Geodynamic Monograph 19, p. 221–234, doi:10.1029/GD019p0221.

Kravchinsky, V., Sorokin, A., and Courtillot, V., 2002a, Paleomagnetism of Paleozoic and Mesozoic sediments of southern margin of Mongol-Okhotsk Ocean: Far East of Russia: Journal of Geophysical Research, v. 107, p. 2253, doi:10.1029/2001JB000672.

Kravchinsky, V.A., Cogné, J.-P., Harbert, W.P., and Kuzmin, M.I., 2002b, Evolution of the Mongol-Okhotsk Ocean as constrained by new palaeomagnetic data from the Mongol-Okhotsk suture zone, Siberia: Geophysical Journal International, v. 148, p. 34–57, doi:10.1046/j.1365-246x.2002.01557.x.

Kurihara, T., Tsukada, K., Otoh, S., Kashiwaga, K., Chuluun, M., Byambadash, D., Boijir, B., Gonchigdorj, S., Nuramkhan, M., Niwa, M., Tokiwa, T., Hikichi, G.Y., and Kozuka, T., 2008, Upper Silurian and Devonian pelagic deep-water radiolarian chert from the Khangai–Khentei belt of central Mongolia: Evidence for middle Paleozoic subduction accretion activity in the Central Asian orogenic belt: Journal of Asian Earth Sciences, v. 34, p. 209–225, doi:10.1016/j.jseaes.2008.04.010.

Kuzmin, M.I., and Kravchinsky, V.A., 1996, First paleomagnetic data for the Mongol-Okhotsk fold belt: Russian Journal of Geology and Geophysics, v. 37, p. 54–62 [in Russian].

Lehmann, J., Schulmann, K., Lexa, O., Corsini, M., Kröner, A., Stípská, P., Tomurhuu, D., and Otgonbator, D., 2010, Structural constraints on the evolution of the Central Asian orogenic belt in SW Mongolia: American Journal of Science, v. 310, p. 575–628, doi:10.2475/07.2010.02.

Li, S., Jagoutz, E., Chen, Y., and Li, Q., 2000, Sm-Nd and Rb-Sr isotopic chronology and cooling history of ultrahigh pressure metamorphic rocks and their country rocks at Shuanghe in the Dabie Mountains, central China: Geochimica et Cosmochimica Acta, v. 64, p. 1077–1093, doi:10.1016/S0016-7037(99)00319-1.

Li, Y., Ali, J.R., Chang, L.S., and Lee, C.M., 2005, New and revised set of Cretaceous paleomagnetic poles from Hong Kong: Implications for the development of southeast China: Journal of Asian Earth Sciences, v. 24, p. 481–493, doi:10.1016/j.jseaes.2004.01.004.

Li, Z.-X., Metcalfe, I., and Wang, X., 1995, Vertical-axis block rotations in southwestern China since the Cretaceous: New paleomagnetic results from Hainan Island: Geophysical Research Letters, v. 22, p. 3071–3074, doi:10.1029/95GL03169.

Lin, J.L., 1984, The apparent polar wander paths for the North and South China blocks [Ph.D. dissertation]: University of California at Santa Barbara, 248 p.

Lin, W., Chen, Y., Faure, M., and Wang, Q., 2003, Tectonic implications of new Late Cretaceous paleomagnetic constraints from eastern Liaoning Peninsula, NE China: Journal of Geophysical Research, v. 108, p. 2313, doi:10.1029/2002JB002169.

Lin, W.Z., Shao, J., and Zhao, Z., 1984, Paleomagnetic features of the Sino-Korea plate in the late Paleozoic: Geophysical and Geochemical Exploration, v. 5, p. 297 [in Chinese].

Liu, J., Yang, Z., Tong, Y., Yuan, W., and Wang, B., 2010, Tectonic implications of Early-Middle Triassic palaeomagnetic results from Hexi corridor, North China: Geophysical Journal International, v. 182, p. 1216–1228, doi:10.1111/j.1365-246X.2010.04699.x.

Liu, Y., and Morinaga, H., 1999, Cretaceous palaeomagnetic results from Hainan Island in South China supporting the extrusion model of Southeast Asia: Tectonophysics, v. 301, p. 133–144, doi:10.1016/S0040-1951(98)00216-9.

Ma, X., Yang, Z., and Xing, L., 1993, The Lower Cretaceous reference pole for North China, and its tectonic implications: Geophysical Journal International, v. 115, p. 323–331, doi:10.1111/j.1365-246X.1993.tb05607.x.

McElhinny, M.W., Embleton, B.J.J., Ma, X.H., and Zhang, Z.K., 1981, Fragmentation of Asia in the Permian: Nature, v. 293, p. 212–216, doi:10.1038/293212a0.

Metelkin, D.V., Gordienko, I.V., and Klimuk, V.S., 2007, Paleomagnetism of Upper Jurassic basalts from Transbaikalia: New data on the time of closure of the Mongol-Okhotsk Ocean and Mesozoic intraplate tectonics

of Central Asia: Russian Geology and Geophysics, v. 48, p. 825–834, doi:10.1016/j.rgg.2007.09.004.

Morinaga, H., and Liu, Y., 2004, Cretaceous paleomagnetism of the eastern South China block: Establishment of the stable body of SCB: Earth and Planetary Science Letters, v. 222, p. 971–988, doi:10.1016/j.epsl.2004.02.035.

Narumoto, K., Yang, Z.Y., Takemoto, K., Zaman, H., Morinaga, H., and Otofuji, Y.-I., 2006, Anomalously shallow inclination in middle-northern part of the South China block: Palaeomagnetic study of Late Cretaceous red beds from Yichang area: Geophysical Journal International, v. 164, p. 290–300, doi:10.1111/j.1365-246X.2005.02820.x.

Natal'in, B.A., 1993, History and modes of Mesozoic accretion in southeastern Russia: The Island Arc, v. 2, p. 15–34, doi:10.1111/j.1440-1738.1993.tb00072.x.

Okay, A.I., Şengör, A.M.C., and Satir, M., 1993, Tectonics of an ultrahigh-pressure metamorphic terrane: The Dabie Shan/Tongbai Shan orogen, China: Tectonics, v. 12, p. 1320–1334.

Pei, P., Sun, Z., Liu, J., Liu, J., Wang, X., Yang, Z., Zhao, Y., and Li, H., 2011, A paleomagnetic study from the Late Jurassic volcanics (155 Ma), North China: Implications for the width of Mongol–Okhotsk Ocean: Tectonophysics, v. 510, p. 370–380, doi:10.1016/j.tecto.2011.08.008.

Roger, F., Arnaud, N., Gilder, S., Tapponnier, P., Jolivet, M., Brunel, M., Malavieille, J., Xu, Z., and Yang, J., 2003, Geochronological and geochemical constraints on Mesozoic suturing in east central Tibet: Tectonics, v. 22, p. 1037, doi:10.1029/2002TC001466.

Sato, S., Yang, Z., Tong, Y., Fujihara, M., Zaman, H., Yokoyama, M., Kitada, K., and Otofuji, Y.-I., 2011, Inclination variation in the Late Jurassic to Eocene red beds from Southeast Asia: Lithological to locality scale approach: Geophysical Journal International, v. 186, p. 471–491, doi:10.1111/j.1365-246X.2011.05030.x.

Şengör, A.M.C., and Atayman, S., 2009, The Permian Extinction and the Tethys: An Exercise in Global Geology: Geological Society of America Special Paper 448, 85 p.

Şengör, A.M.C., and Natal'in, B.A., 1996, Paleotectonics of Asia: Fragments of a synthesis, *in* Yin, A., and Harrison, T.M., eds., The Tectonic Evolution of Asia: Cambridge, UK, Cambridge University Press, p. 486–640.

Şengör, A.M.C., Natal'in, B.A., and Burtman, V.S., 1993, Evolution of the Altaid tectonic collage and Palaeozoic crustal growth in Eurasia: Nature, v. 364, p. 299–306.

Shaw, J., Johnston, S.T., Gutiérrez-Alonso, G., and Weil, A.B., 2012, Oroclines of the Variscan orogen of Iberia: Paleocurrent analysis and paleogeographic implications: Earth and Planetary Science Letters, v. 329–330, p. 60–70, doi:10.1016/j.epsl.2012.02.014.

Steinberger, B., and Torsvik, T.H., 2008, Absolute plate motions and true polar wander in the absence of hotspot tracks: Nature, v. 452, p. 620–623, doi:10.1038/nature06824.

Sun, Z., Yang, Z., Yang, T., Pei, J., and Yu, Q., 2006, New Late Cretaceous and Paleogene paleomagnetic results from South China and their geodynamic implications: Journal of Geophysical Research, v. 111, p. B03101, doi:10.1029/2004JB003455.

Tomurtogoo, O., Windley, B.F., Kröner, A., Badarch, G., and Liu, D.Y., 2005, Zircon age and occurrence of the Adaatsag ophiolite and Muron shear zone, central Mongolia: Constraints on the evolution of the Mongol-Okhotsk Ocean, suture and orogen: Journal of the Geological Society of London, v. 162, p. 125–134, doi:10.1144/0016-764903-146.

Torsvik, T.H., and Cocks, L.R.M., 2004, Earth geography from 400 to 250 Ma: A paleomagnetic, faunal and facies review: Journal of the Geological Society of London, v. 161, p. 555–572, doi:10.1144/0016-764903-098.

Torsvik, T.H., Müller, R.D., Van der Voo, R., Steinberger, B., and Gaina, C., 2008a, Global plate motion frames: Toward a unified model: Reviews of Geophysics, v. 46, p. RG3004, doi:10.1029/2007RG000227.

Torsvik, T.H., Steinberger, B., Cocks, L.R.M., and Burke, K., 2008b, Longitude: Linking Earth's ancient surface to its deep interior: Earth and Planetary Science Letters, v. 276, p. 273–282, doi:10.1016/j.epsl.2008.09.026.

Torsvik, T.H., Burke, K., Webb, S., Ashwal, L., and Steinberger, B., 2010, Diamonds sampled by plumes from the core-mantle boundary: Nature, v. 466, p. 352–355, doi:10.1038/nature09216.

Torsvik, T.H., Van der Voo, R., Preeden, U., Mac Niocaill, C., Steinberger, B., Doubrovine, P.V., van Hinsbergen, D.J.J., Domeier, M., Gaina, C., Tohver, E., Meert, J.G., McCausland, P.J.A., and Cocks, L.R.M., 2012, Phanerozoic polar wander, paleogeography and dynamics: Earth-Science Reviews, v. 114, p. 325–368, doi:10.1016/j.earscirev.2012.06.007.

Tsuneki, Y., Morinaga, H., and Liu, Y., 2009, New palaeomagnetic data supporting the extent of the stable body of the South China block since the Cretaceous and some implications on magnetization acquisition of red beds: Geophysical Journal International, v. 178, p. 1327–1336, doi:10.1111/j.1365-246X.2009.04222.x.

Uno, K., 2000, Clockwise rotation of the Korean Peninsula with respect to the North China block inferred from an improved Early Triassic palaeomagnetic pole for the Ryeongnam block: Geophysical Journal International, v. 143, p. 969–976, doi:10.1046/j.0956-540X.2000.01289.x.

Uno, K., and Huang, B., 2003, Constraints on the Jurassic swing of the apparent polar wander path for the North China block: Geophysical Journal International, v. 154, p. 801–810, doi:10.1046/j.1365-246X.2003.01992.x.

van der Beek, P., Delvaux, D., Andriessen, P., and Levi, K., 1996, Early Cretaceous denudation related to convergent tectonics in the Baikal region, SE Siberia: Journal of the Geological Society of London, v. 153, p. 515–523, doi:10.1144/gsjgs.153.4.0515.

van der Meer, D.G., Spakman, W., van Hinsbergen, D.J.J., Amaru, M.L., and Torsvik, T.H., 2010, Toward absolute plate motions constrained by lower mantle slab remnants: Nature Geoscience, v. 3, p. 36–40, doi:10.1038/ngeo708.

van der Meer, D.G., Torsvik, T.H., Spakman, W., van Hinsbergen, D.J.J., and Amaru, M.L., 2012, Triassic–Jurassic subduction zones within the Panthalassa Ocean revealed by fossil arcs and mantle structure: Nature Geoscience, v. 5, p. 215–219, doi:10.1038/ngeo1401.

Van der Voo, R., Spakman, W., and Bijwaard, H., 1999, Mesozoic subducted slabs under Siberia: Nature, v. 397, p. 246–249, doi:10.1038/16686.

van Hinsbergen, D.J.J., Straathof, G.B., Kuiper, K.F., Cunningham, W.D., and Wijbrans, J.R., 2008, No rotations during transpressional orogeny in the Gobi Altai: Coinciding Mongolian and Eurasian apparent polar wander paths: Geophysical Journal International, v. 173, p. 105–126, doi:10.1111/j.1365-246X.2007.03712.x.

Wang, B., and Yang, Z., 2007, Late Cretaceous paleomagnetic results from southeastern China, and their geological implication: Earth and Planetary Science Letters, v. 258, p. 315–333, doi:10.1016/j.epsl.2007.03.045.

Wilhem, C., Windley, B.F., and Stampfli, G.M., 2012, The Altaids of Central Asia: A tectonic and evolutionary innovative review: Earth-Science Reviews, v. 113, p. 303–341, doi:10.1016/j.earscirev.2012.04.001.

Windley, B.F., Alexeiev, D., Xiao, W., Kröner, A., and Badarch, G., 2007, Tectonic models for accretion of the Central Asian orogenic belt: Journal of the Geological Society of London, v. 164, p. 31–47, doi:10.1144/0016-76492006-022.

Wu, H., Chang, C.F., Liu, C., and Zhong, D.L., 1990, A paleomagnetic study of the movement of SCB and NCB and its implications for the evolution of the Qinling orogenic belt: Scientia Geologica Sinica, v. 3, p. 201–213 [in Chinese].

Wu, H., Zhu, R., Courtillot, V., Bai, L., Zhao, Y., and Yang, G., 1999, Paleomagnetic results of Paleozoic and Mesozoic rocks from Xingshan-Zigui section in Hubei Province, South China: Science in China, Earth Science, v. 42, p. 182–194.

Wysession, M.E., 1996, Imaging cold rock at the base of the mantle: The sometimes fate of slabs?, *in* Bebout, G., Scholl, D.W., Kirby, S.H., and Platt, J.P., eds., Subduction Top to Bottom: American Geophysical Union Geophysical Monograph 96, p. 369–384, doi:10.1029/GM096p0369.

Xiao, W.J., Windley, B.F., Huang, B.C., Han, C.M., Yuan, C., Chen, H.L., Sun, M., Sun, S., and Li, J.L., 2009, End-Permian to mid-Triassic termination of the accretionary processes of the southern Altaids: Implications for geodynamic evolution, Phanerozoic continental growth, and metallogeny of Central Asia: International Journal of Earth Sciences, v. 98, p. 1189–1217, doi:10.1007/s00531-008-0407-z.

Xiao, W.J., Huang, B., Han, C., Sun, S., and Li, J., 2010, A review of the western part of the Altaids: A key to understanding the architecture of accretionary orogens: Gondwana Research, v. 18, p. 253–273, doi:10.1016/j.gr.2010.01.007.

Xu, X., Harbert, W., Dril, S., and Kravchinsky, V., 1997, New paleomagnetic data from the Mongol-Okhotsk collision zone, Chita region, south-central Russia: Implications for Paleozoic paleogeography of the Mongol-Okhotsk Ocean: Tectonophysics, v. 269, p. 113–129, doi:10.1016/S0040-1951(96)00140-0.

Yakubchuk, A., 2004, Architecture and mineral deposit settings of the Altaid orogenic collage: A revised model: Journal of Asian Earth Sciences, v. 23, p. 761–779, doi:10.1016/j.jseaes.2004.01.006.

Yakubchuk, A., 2008, Re-deciphering the tectonic jigsaw puzzle of northern Eurasia: Journal of Asian Earth Sciences, v. 32, p. 82–101, doi:10.1016/j .jseaes.2007.10.009.

Yan, M.D., Fang, X.M., Van der Voo, R., Song, C.H., and Li, J.J., 2013, Neogene rotations in the Jiuquan Basin, Hexi corridor, China, *in* Jovane, L., Herrero-Bervera, E., Hinnov, L.A., and Housen, B.A., eds., Magnetic Methods and the Timing of Geological Processes: Geological Society of London Special Publication 373, p. 173–189.

Yang, Z., and Besse, J., 2001, New Mesozoic apparent polar wander path for South China: Tectonic consequences: Journal of Geophysical Research, v. 106, p. 8493–8520, doi:10.1029/2000JB900338.

Yang, Z., Ma, X., Besse, J., Courtillot, V., Xing, L., Xu, S., and Zhang, J., 1991, Paleomagnetic results from Triassic sections in the Ordos Basin, North China: Earth and Planetary Science Letters, v. 104, p. 258–277, doi:10.1016/0012-821X(91)90208-Y.

Yang, Z., Courtillot, V., Besse, J., Ma, X., Xing, L., Xu, S., and Zhang, J., 1992, Jurassic paleomagnetic constraints on the collision of the North and South China blocks: Geophysical Research Letters, v. 19, p. 577–580, doi:10.1029/91GL02416.

Yokoyama, M., Liu, Y., Otofuji, Y.-I., and Yang, Z., 1999, New Late Jurassic palaeomagnetic data from the northern Sichuan Basin: Implications for the deformation of the Yangtze craton: Geophysical Journal International, v. 139, p. 795–805, doi:10.1046/j.1365-246x.1999.00951.x.

Yokoyama, M., Liu, Y., Halim, N., and Otofuji, Y.-I., 2001, Paleomagnetic study of Upper Jurassic rocks from the Sichuan Basin: Tectonic aspects for the collision between the Yangtze block and the North China block: Earth and Planetary Science Letters, v. 193, p. 273–285, doi:10.1016/ S0012-821X(01)00498-8.

Zhai, Y., Seguin, M.-K., Zhou, Y., Dong, J., and Zheng, Y., 1992, New paleomagnetic data from the Huanan block, China, and Cretaceous tectonics in eastern China: Physics of the Earth and Planetary Interiors, v. 73, p. 163–188, doi:10.1016/0031-9201(92)90088-D.

Zhao, X., and Coe, R.S., 1989, Tectonic implications of Permo-Triassic paleomagnetic results from North and South China, *in* Hillhouse, J.W., ed., Deep Structure and Past Kinematics of Accreted Terranes: American Geophysical Union Geophysical Monograph 50, p. 267–283.

Zhao, X., Coe, R.S., Zhou, Y., Wu, H., and Wang, J., 1990, New paleomagnetic results from northern China: Collision and suturing with Siberia and Kazakhstan: Tectonophysics, v. 181, p. 43–81, doi:10.1016/0040-1951(90)90008-V.

Zheng, Z., Kono, M., Tsunakawa, H., Kimura, G., Wei, Q., Zhu, X., and Hao, T., 1991, The apparent polar wander path for the North China block since the Jurassic: Geophysical Journal International, v. 104, p. 29–40.

Zhu, R., Pan, Y., Shaw, J.H., Li, D., and Li, Q., 2001, Geomagnetic palaeointensity just prior to the Cretaceous normal superchron: Physics of the Earth and Planetary Interiors, v. 128, p. 207–222, doi:10.1016/S0031 -9201(01)00287-4.

Zhu, Z., Hao, T., and Zhao, H., 1988, Paleomagnetic study on the tectonic evolution of Pan-Xi block and adjacent area during YinZhi-Yanshan period: Acta Geophysica Sinica, v. 41, p. 420–431 [in Chinese].

Zhu, Z., Morinaga, H., Gui, R., Xu, S., and Liu, Y., 2006, Paleomagnetic constraints on the extent of the stable body of the South China block since the Cretaceous: New data from the Yuanma Basin, China: Earth and Planetary Science Letters, v. 248, p. 533–544, doi:10.1016/j.epsl.2006.06.029.

Zonenshain, L.P., Kuzmin, M.I., Natapov, L.M., and Page, B.J., eds., 1990, Geology of the USSR: A Plate Tectonic Synthesis: American Geophysical Union Geodynamic Monograph 21, 240 p., doi:10.1029/GD021.

Zorin, Y.A., 1999, Geodynamics of the western part of the Mongolia-Okhotsk collisional belt, Trans-Baikal region (Russia) and Mongolia: Tectonophysics, v. 306, p. 33–56, doi:10.1016/S0040-1951(99)00042-6.